

Solving Inverse Problems with REINFORCE

Chen Xu¹, Zhipeng Lu¹, and Ye Zhang^{*2,3}

¹Guangdong Laboratory of Machine Perception and Intelligent Computing,
Shenzhen MSU-BIT University, China.

²Faculty of Computational Mathematics and Cybernetics, Shenzhen
MSU-BIT University, 518172 Shenzhen, China

³School of Mathematics and Statistics, Beijing Institute of Technology,
100081 Beijing, China

Email: {xuchen, zhipeng.lu, ye.zhang}@smbu.edu.cn

Abstract

In this paper, with rigorous derivations we formally introduce the usage of reinforcement learning to the field of inverse problems by designing an iterative algorithm, called REINFORCE-IP, for solving a general type of non-linear inverse problems. By setting specific probability densities of the action rule, we connect our approach to the conventional regularization methods of Tikhonov regularization and iterative regularization. For the numerical implementation of our approach, we parameterize the solution-searching rule with the help of neural networks and iteratively improve the parameter using a reinforcement learning algorithm – REINFORCE. Under standard assumptions we prove the almost sure convergence of the parameter to a locally optimal value. Our work provides two typical examples (nonlinear integral equations and parameter identification problems in partial differential equations) on how reinforcement learning can be applied in solving non-linear inverse problems. Our numerical experiments show that REINFORCE-IP is an efficient algorithm that can escape from local minimums and identify multi-solutions for inverse problems with non-uniqueness.

1 Introduction

In this paper, we study the theory of using a reinforcement learning (RL) algorithm to search for an iterative method to solve the following general inverse problem:

(IP) Given a sequence of sample data $\{\mathbf{y}_k^\delta\}_{k=1}^K$ of random variable \mathbf{y}^δ , estimate the solution \mathbf{x}_e of the operator equation of population model

$$f(\mathbf{x}_e) + \delta\xi = \mathbf{y}^\delta, \quad (1)$$

where $f : \mathcal{H}_1 \supset \mathcal{D}(f) \rightarrow \mathcal{H}_2$ is a map between two Hilbert spaces, $\delta > 0$ denotes the noise level and ξ represents a Hilbert space process¹ on \mathcal{H}_2 . Rigorously, problem (1) can

*Corresponding author

¹A Hilbert space process ξ is a bounded linear mapping $\xi : \mathcal{H}_2 \rightarrow L^2(\Omega, \mathcal{A}, P)$ with a probability space (Ω, \mathcal{A}, P) .

be understood as follows: for each $z \in \mathcal{H}_2$, one has the access to the value of $\langle \mathbf{y}^\delta, z \rangle$ that satisfies

$$\langle f(\mathbf{x}_e), z \rangle + \delta \langle \xi, z \rangle = \langle \mathbf{y}^\delta, z \rangle,$$

where for simplicity we denote by $\langle \cdot, \cdot \rangle$ the inner products for both Hilbert spaces. The noise term $\xi_z := \langle \xi, z \rangle$, i.e. ξ can be interpreted as a random element in the algebraic dual space of \mathcal{H}_2 . Model (1) includes the standardized Gaussian white noise model where $\xi_z \sim N(0, \|z\|_{\mathcal{H}_2}^2)$ and $\text{Cov}[\xi_{z_1}, \xi_{z_2}] = \langle z_1, z_2 \rangle$ for all $z_1, z_2 \in \mathcal{H}_2$, where $\|\cdot\|$ denotes the norm in the Hilbert space.

For ill-posed problems², a variant of regularization is required for finding stable approximations to the solution \mathbf{x}_e of inverse problem (1), and we exploit in this context a variant of Tikhonov variational regularization with regularization term $\Omega(\mathbf{x})$ and regularization parameter $\alpha > 0$, where the regularized solution \mathbf{x}_α^δ is a solution to the following problem

$$\min_{\mathbf{x}} \frac{1}{K} \sum_{k=1}^K \|f(\mathbf{x}) - \mathbf{y}_k^\delta\|^2 + \alpha \Omega(\mathbf{x}). \quad (2)$$

There are two drawbacks for the formulation (2):

- (a) The estimator \mathbf{x}_α^δ is deterministic, and it can not be used to qualify the uncertainty caused by the noise;
- (b) There exists no efficient numerical algorithm for solving (2) if it is non-convex (i.e., it has more than one local minimums) or if f is non-differentiable. Such cases are often encountered in practice.

In order to address the first issue (a), in this work, instead of conventional deterministic formulation (2), we consider a statistical formulation: the designed regularization solution \mathbf{x} is a random variable, following the distribution d^{π_θ} with parameters $\theta = \hat{\theta}$, which are determined according to the following optimization problem

$$\hat{\theta} = \arg \min_{\theta} \mathbb{E}_{\mathbf{y}^\delta} \mathbb{E}_{\mathbf{x} \sim d^{\pi_\theta}} [\|f(\mathbf{x}) - \mathbf{y}^\delta\|^2 + \alpha \Omega(\mathbf{x}) + \beta \|\theta\|_w^2] \quad (3)$$

with double regularization penalties, where the parameterized distribution d^{π_θ} and the weighted Euclidean norm $\|\cdot\|_w$ will be explained or specified later in Section 2.1 and 2.2, respectively. As studied in [35, Section 2.2] and demonstrated example in Section 5.1 later, such random element \mathbf{x} can be used to quantify the uncertainty in error estimates for inverse problems.

Furthermore, in order to solve the second trouble (b), in this work, we formulate the inverse problem (1) with a Markov decision process (MDP) setting (which can be understood as a finite approximation of the formulation (3)), and solve it using a popular reinforcement learning algorithm called REINFORCE. The motivation of using reinforcement learning (RL) rather than other methods (e.g., gradient descents and supervised learning) for solving inverse problems is because RL is free of issue (b) associated with those methods. Specifically, (i) the forward map f is not required to be differentiable (e.g., see the REINFORCE algorithm 21) so that the cases where f' is difficult to compute or even does not exist can be handled. (ii) The produced trajectory $\{\mathbf{x}_t\}$ by the found updating rule π_{θ^*} may escape from the local minimum of objective functional $\|f(\mathbf{x}) - \mathbf{y}^\delta\|^2$ since π_{θ^*} is not designed based on f' . For visualization of this observation, Figure 1 and 2 illustrates the capability of an RL algorithm called REINFORCE to escape from the local minimum of a

²We refer to in the sense of [15, Def. 1.1] and [14, Def. 3] for a rigorous definition of (locally) ill-posedness of a nonlinear operator equation .

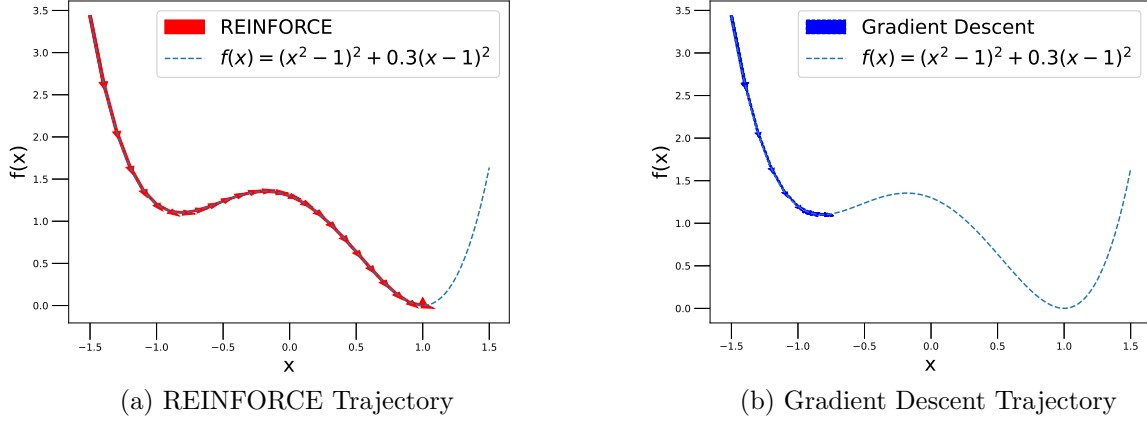


Figure 1: Illustration: REINFORCE escapes from the local minimum. The problem to solve is $\min_{x \in \mathbb{R}} f(x)$ with $f(x) = (x^2 - 1)^2 + 0.3(x - 1)^2$ and the initial value $x_0 = -1.5$. It looks like the gradient descent agent moves only two steps. But in fact it keeps moving back and forth around the local minimum.

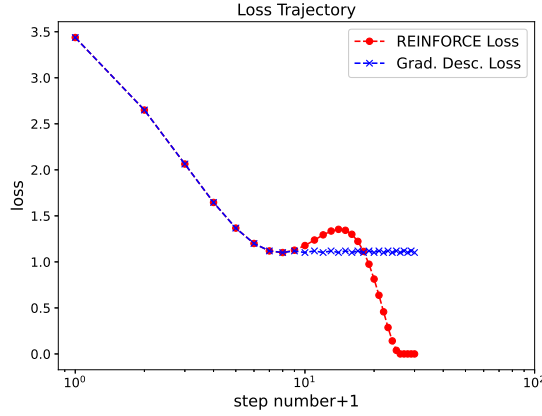


Figure 2: The loss trajectory of the two methods in Figure 1, where the loss at step n is set as $f(x_n)$.

given simple non-linear function $f(x) = (x^2 - 1)^2 + 0.3(x - 1)^2$. (iii) The RL algorithm is also able to deal with the multiple-solutions case of Eq. (1) while the commonly used supervised learning framework like neural networks cannot be used to model the multi-valued inversion map f^{-1} directly (e.g., [31, 33]). This observation will be demonstrated in our first numerical experiments in Section 5.1.

Essentially, it can be viewed that REINFORCE parameterizes the distribution of \mathbf{x} with a pre-selected functional form $d^{\pi_{\theta}}$ and then searches for θ that minimizes the objective functional in (3). This idea is similar to that of regularized maximal-likelihood estimation (MLE)³ that aims to find a \mathbf{x} -distribution so that the probability of the observed \mathbf{y}^{δ} is maximized. However, some technical difficulties for MLE are avoided by REINFORCE. For instance, if $f(\cdot)$ is assumed to have a non-linear form, given the distribution of \mathbf{x} it is generally difficult or even impossible to obtain the distribution of $f(\mathbf{x})$, which is required by MLE to derive the probability of the observed \mathbf{y}^{δ} . REINFORCE is free of this issue and

³The MLE scheme pre-selects a distribution for \mathbf{x} parameterized with some parameter θ , and derive the distribution of $f(\mathbf{x})$ which is then used to compute the probability $p_{\theta}(\mathbf{y}^{\delta})$ of the observed \mathbf{y}^{δ} . Then, it solves $\max_{\theta} \log p_{\theta}(\mathbf{y}^{\delta})$.

applies universally comparing to MLE.

We highlight the essential contributions of our work in the following:

- We introduce in a mathematical way a RL algorithm to the field of inverse problems. RL is originally designed for the type of problems that are seemingly different from (1), which aim to find a series of actions for an agent traveling in a dynamic environment to maximize the resulting rewards. This work provides a first connection between RL and classical regularization methods (i.e. both variational and iterative regularization methods) for solving general inverse problems (1), cf. Section 2.
- The widely-used algorithm ([34, 23, 38]) – REINFORCE is firstly proposed in [30], where its convergence analysis is not provided. We rigorously prove that with standard assumptions, REINFORCE produces a sequence $\{\theta_t\}_{t=0}^\infty$ that almost surely converges to a locally optimal value. The main result is in our Theorem 1 and we use the ordinary-differential-equation method (e.g., [6] and [4, Section 8.1]) in our proof.
- We are the first to prove in theory that an RL algorithm converges to a x_t -iteration method for solving (1). Existing researches that apply RL to inverse problems are few, and they focus on the empirical application of RL algorithms. For example, [28] uses deep RL⁴ to solve a physical chemistry problem – to invert nuclear magnetic resonance spectra for molecular structures. [9] designs an inversion algorithm based on Q-learning and applies it to a problem in geosciences. [27] states on how to transform the Bayesian sequential optimal experimental design, a method for solving inverse problems, to a problem that can be solved by RL.
- Our numerical experiments show that the REINFORCE algorithm is capable for solving (1) with complicated function f , indicating REINFORCE is a practical and successful method for inverse problems.

The remainder of the paper is structured as follows: Section 2 frames the inverse problem in 1 with an MDP setting, and then discusses the connections between the MDP formulation and conventional regularization methods. Section 3 presents the main results of this work, including the main algorithm, assumptions and convergence results. The proof details of main theorem are given in Section 4. Section 5 shows the performance of REINFORCE with numerical examples of non-linear integral equations and parameter identification problems of a nonlinear time dependent partial differential equations. Finally, concluding remarks are given in Section 6, and some technical proofs of assertions are provided in the Appendices.

2 Connection between RL and classical regularization methods

2.1 Formulation of Inverse Problem (1) in the MDP setting

Above all, let us formulate (1) in a MDP setting⁵ so that RL algorithms can be applied as an iterative method to solve it. As we will show, such iterative method can be interpreted as iterative regularization for solving inverse problems (1).

⁴Deep RL uses deep neural networks as approximators in RL algorithms. See [24] for more details on the deep RL.

⁵A MDP is featured with an agent that takes a series of actions in a dynamical environment and receives a series of rewards which are determined by the state-action pairs. Each action is taken based only on the current state (independently from the past states and actions), which is the Markov property. For more details on MDP, we refer the reader to [29, Section 3.1]

Suppose that there is an agent traveling in \mathcal{H}_1 and his location is the state. At each time t the agent takes a step (action $\mathbf{a}_t \in \mathcal{H}_1$) from the current state \mathbf{x}_t , reaches to a new state $\mathbf{x}_{t+1} = \mathbf{x}_t + \mathbf{a}_t$, and receives a reward $R(\mathbf{x}_t, \mathbf{a}_t)$.

RL algorithms aim to find the \mathbf{a}_t -selection rule π (time-independent), which is a map from the \mathbf{x} -space \mathcal{S} to the set of probability distributions $PD(\mathcal{A})$ over the \mathbf{a} -space \mathcal{A} , that maximizes the expected average rewards⁶. After parameterizing the policy with $\pi_{\boldsymbol{\theta}}$, they aim to solve

$$\max_{\boldsymbol{\theta} \in \mathbb{R}^d} \{J_T(\boldsymbol{\theta}) - \beta \|\boldsymbol{\theta}\|_w^2\}, \quad (4)$$

where $\beta > 0$ is the regularization coefficient, $\|\cdot\|_w$ denotes the weighted Euclidean norm, i.e., $\|\boldsymbol{\theta}\|_w^2 = \sum_{i=1}^d w_i \theta_i^2$ with positive numbers w_i ,

$$J_T(\boldsymbol{\theta}) := \frac{1}{T} \sum_{t=0}^{T-1} \mathbb{E}_{\mathbf{x}_t, \mathbf{a}_t} [R(\mathbf{x}_t, \mathbf{a}_t) | \pi_{\boldsymbol{\theta}}], \quad (5)$$

and

- $\pi_{\boldsymbol{\theta}}(\cdot | \mathbf{x})$ is a distribution over the action space determined by the current state \mathbf{x} .
- $\mathbf{x}_t \in \mathcal{S}$ denotes the t^{th} step's state and $\mathcal{S} \subset \mathcal{H}_1$ is called the state space.
- $\mathbf{a}_t \in \mathcal{A}$ denotes the agent's t^{th} action and $\mathcal{A} \subset \mathcal{H}_1$ is called the action space. The distribution of \mathbf{a}_t is $\pi_{\boldsymbol{\theta}}(\cdot | \mathbf{x}_t)$.
- $\mathbb{E}_{\mathbf{x}_t, \mathbf{a}_t} [\cdot | \pi_{\boldsymbol{\theta}}]$ denotes an expectation with respect to $(\mathbf{x}_t, \mathbf{a}_t)$, where $(\mathbf{x}_t, \mathbf{a}_t)$ is the t^{th} step state-action pair of a trajectory generated following $\pi_{\boldsymbol{\theta}}$. Note that the distribution of the initial state \mathbf{x}_0 is independent from $\pi_{\boldsymbol{\theta}}$. It is determined by the problem environment or set by the user.
- The transition rule from a state-action pair to the next state is

$$\mathbf{x}_{t+1} = \mathbf{x}_t + \mathbf{a}_t. \quad (6)$$

We remark that the transition rule can be set differently for a general problem. Nevertheless, we adopt (6) throughout this paper since it is proper for the inverse problem (1).

- The reward function R is defined so that solving (4) is equivalent to finding a \mathbf{a}_t -selection rule π ($\Delta \mathbf{x}_t$ -selection rule) such that the agent will reach \mathbf{x}_e as soon as possible. There are multiple options for the functional form of R . For example, a non-linear one can be

$$R(\mathbf{x}, \mathbf{a}) := -\mathbb{E}_{\mathbf{y}^\delta} [\|f(\mathbf{x} + \mathbf{a}) + \mathbf{y}^\delta\|^2 - \alpha \Omega(\mathbf{x})], \quad (7)$$

or

$$R(\mathbf{x}, \mathbf{a}) := \mathbb{E}_{\mathbf{y}^\delta} \left[\frac{1}{\|f(\mathbf{x} + \mathbf{a}) - \mathbf{y}^\delta\|^2 + 0.001 + \alpha \Omega(\mathbf{x})} \right], \quad (8)$$

where $\mathbb{E}_{\mathbf{y}^\delta}$ denotes the expectation over the random measurement \mathbf{y}^δ , $\Omega(\cdot)$ denotes a general convex regularization term, and $\alpha > 0$ is the regularization parameter. The number 0.001 is added to avoid a zero-denominator.

⁶See [29, Eq.(13.15)] for the definition of a long-term performance measure. Another common way of defining the performance measure is the expected sum of discounted rewards, i.e., $J(\pi) := \mathbb{E}_{\mathbf{a}_t \sim \pi(\mathbf{x}_t)} \left[\lim_{T \rightarrow \infty} \sum_{t=0}^T \gamma^t R(\mathbf{x}_t, \mathbf{a}_t) \right]$, where $\gamma \in (0, 1]$ is the discount factor.

- $T \in \mathbb{Z}^+$ is the pre-selected number of steps.

Therefore, RL can be viewed as a method for finding an \mathbf{x}_t -iteration rule to solve (1). Throughout the paper, a trajectory generated by the policy π_θ refers to $\{(\mathbf{x}_t, \mathbf{a}_t)\}_{t=0}^{T-1}$ where \mathbf{x}_0 is sampled from a distribution that is potentially independent from π_θ , $\mathbf{a}_t \sim \pi_\theta(\cdot|\mathbf{x}_t)$, and $\mathbf{x}_{t+1} = \mathbf{x}_t + \mathbf{a}_t$. We also call $\{\mathbf{x}_t\}_{t=0}^{T-1}$ in the trajectory as generated by π_θ . It is not difficult to see that $\{\mathbf{x}_t\}$ is a Markov chain if we let $T \rightarrow +\infty$.

2.2 Interpreting $J_T(\theta)$

Without loss of generality, we assume in this subsection that \mathcal{S} is a discrete space. For the continuous case, we only need to change the summation Σ to an integral in the following interpretation.

Suppose⁷ that for any $\theta \in \mathbb{R}^d$ the Markov chain $\{\mathbf{x}_t\}$ generated following the policy π_θ has a stationary distribution d^{π_θ} , i.e., for any $\mathbf{x} \in \mathcal{S}$ we have

$$\lim_{t \rightarrow \infty} p(\mathbf{x}_t = \mathbf{x}|\pi_\theta) = d^{\pi_\theta}(\mathbf{x}),$$

which further implies (even if $p(\mathbf{x}_t = \mathbf{x}|\pi_\theta)$ changes with t)

$$\lim_{T \rightarrow +\infty} \frac{1}{T} \sum_{t=0}^{T-1} p(\mathbf{x}_{t+1} = \mathbf{x}|\pi_\theta) = d^{\pi_\theta}(\mathbf{x}). \quad (9)$$

Then, we apply the above result in the second to last step of the following derivation.

$$\begin{aligned} \lim_{T \rightarrow +\infty} J_T(\theta) &= \lim_{T \rightarrow +\infty} \frac{1}{T} \sum_{t=0}^{T-1} \mathbb{E}_{\mathbf{x}_t, \mathbf{a}_t} [R(\mathbf{x}_t, \mathbf{a}_t)|\pi_\theta] \\ &= - \lim_{T \rightarrow +\infty} \mathbb{E}_{\mathbf{y}^\delta} \left[\frac{1}{T} \sum_{t=0}^{T-1} \mathbb{E}_{\mathbf{x}_t, \mathbf{a}_t} [\|f(\mathbf{x}_t + \mathbf{a}_t) - \mathbf{y}^\delta\|^2 + \alpha \Omega(\mathbf{x}_t)|\pi_\theta] \right], \text{ by (7),} \\ &= - \lim_{T \rightarrow +\infty} \mathbb{E}_{\mathbf{y}^\delta} \left[\frac{1}{T} \sum_{t=0}^{T-1} (\mathbb{E}_{\mathbf{x}_{t+1}} [\|f(\mathbf{x}_{t+1}) - \mathbf{y}^\delta\|^2|\pi_\theta] + \alpha \mathbb{E}[\Omega(\mathbf{x}_t)|\pi_\theta]) \right] \\ &= - \lim_{T \rightarrow +\infty} \mathbb{E}_{\mathbf{y}^\delta} \left[\frac{1}{T} \sum_{t=0}^{T-1} \sum_{\mathbf{x} \in \mathcal{S}} (p(\mathbf{x}_{t+1} = \mathbf{x}|\pi_\theta) \|f(\mathbf{x}) - \mathbf{y}^\delta\|^2 + p(\mathbf{x}_t = \mathbf{x}|\pi_\theta) \alpha \Omega(\mathbf{x})) \right] \\ &= - \mathbb{E}_{\mathbf{y}^\delta} \left[\sum_{\mathbf{x} \in \mathcal{S}} \|f(\mathbf{x}) - \mathbf{y}^\delta\|^2 \lim_{T \rightarrow +\infty} \frac{1}{T} \sum_{t=0}^{T-1} p(\mathbf{x}_{t+1} = \mathbf{x}|\pi_\theta) \right. \\ &\quad \left. + \sum_{\mathbf{x} \in \mathcal{S}} \alpha \Omega(\mathbf{x}) \lim_{T \rightarrow +\infty} \frac{1}{T} \sum_{t=0}^{T-1} p(\mathbf{x}_t = \mathbf{x}|\pi_\theta) \right] \\ &= - \mathbb{E}_{\mathbf{y}^\delta} \left[\sum_{\mathbf{x} \in \mathcal{S}} (\|f(\mathbf{x}) - \mathbf{y}^\delta\|^2 + \alpha \Omega(\mathbf{x})) d^{\pi_\theta}(\mathbf{x}) \right], \text{ by (9)} \\ &= - \mathbb{E}_{\mathbf{y}^\delta} [\mathbb{E}_{\mathbf{x} \sim d^{\pi_\theta}} [\|f(\mathbf{x}) - \mathbf{y}^\delta\|^2 + \alpha \Omega(\mathbf{x})]], \end{aligned}$$

where \mathbf{x}_{t+1} is the $(t+1)^{th}$ state of a trajectory generated following π_θ , $p(\mathbf{x}_{t+1} = \mathbf{x}|\pi_\theta)$ denotes the probability mass for $\mathbf{x}_{t+1} = \mathbf{x}$, and the interchange between the limit and $\mathbb{E}_{\mathbf{y}^\delta}$

⁷Conditions that ensure the existence of a stationary distribution of $\{\mathbf{x}_t\}$ can be found in Appendix 3. To adapt to the conditions, we can rewrite $\mathbf{x}_{t+1} = \mathbf{x}_t + \mathbf{a}_t = \mathbf{x}_t + \mathbf{m}_\theta(\mathbf{x}_t) + \mathbf{z}_{t+1} = f(\mathbf{x}_t, \mathbf{z}_{t+1})$, where $\mathbf{m}_\theta(\mathbf{x}_t)$ denotes the mean of $\pi_\theta(\cdot|\mathbf{x}_t)$ and $\{\mathbf{z}_t\}$ is a sequence of i.i.d. random variables and $\pi_\theta(\cdot)$ is a deterministic map.

in the fifth line is justified by Lebesgue's dominated convergence theorem. Therefore, if we let $T \rightarrow +\infty$ in (4), this RL goal becomes

$$\max_{\boldsymbol{\theta}} \{-\mathbb{E}_{\mathbf{y}^\delta} \mathbb{E}_{\mathbf{x} \sim d^{\pi_{\boldsymbol{\theta}}}} [\|f(\mathbf{x}) - \mathbf{y}^\delta\|^2 + \alpha \Omega(\mathbf{x}) + \beta \|\boldsymbol{\theta}\|_w^2]\}. \quad (10)$$

Next, we give two examples to explain the connection between this RL goal and the Inverse Problem (1). For simplicity, suppose that we have only a single measurement data \mathbf{y}^δ , which is nonrandom.

2.3 Example I: reinforcement learning goal (10) yields Tikhonov regularization

Consider the linear inverse problems $f(\mathbf{x}) = A\mathbf{x}$, where $A : \mathbb{R}^p \rightarrow \mathbb{R}^q$ is a linear operator for some $p, q \in \mathbb{Z}^+$. We show that $\pi_{\boldsymbol{\theta}^*}$ produces $\{\mathbf{x}_t\}$ that approaches as $t \rightarrow +\infty$ the Tikhonov solution to this linear inverse problem, where the policy π is set as the form below and $\boldsymbol{\theta}^*$ denotes the solution to (10) with $\Omega(\mathbf{x}) = \|\mathbf{x}\|^2$ and $\beta = 0$:

$$\pi_{\boldsymbol{\theta}}(\cdot|\mathbf{x}) := \mathcal{N}(\boldsymbol{\theta} - \mathbf{x}, \Sigma), \quad \text{for any } \mathbf{x} \in \mathcal{S} := \mathbb{R}^q, \quad (11)$$

where \mathcal{N} denotes a Gaussian distribution, $\boldsymbol{\theta} \in \mathbb{R}^q$, and $\Sigma \in \mathbb{R}^{q \times q}$ is a pre-selected symmetric positive definite matrix.

With the form of $\pi_{\boldsymbol{\theta}}$ in Eq. (11), the invariant distribution $d^{\pi_{\boldsymbol{\theta}}}$ is $\mathcal{N}(\boldsymbol{\theta}, \Sigma)$ (The proof will be postponed to the end of this subsection). With this information we rewrite (10):

$$\begin{aligned} & \min_{\boldsymbol{\theta}} \mathbb{E}_{\mathbf{x} \sim d^{\pi_{\boldsymbol{\theta}}}} [\|A\mathbf{x} - \mathbf{y}^\delta\|^2 + \alpha \|\mathbf{x}\|^2] \\ &= \min_{\boldsymbol{\theta}} \|\mathbb{E} A\mathbf{x} - \mathbf{y}^\delta\|^2 + \mathbb{E} \|A\mathbf{x} - \mathbb{E} A\mathbf{x}\|^2 + \alpha \mathbb{E} \|\mathbf{x} - \mathbb{E} \mathbf{x}\|^2 + \alpha \|\mathbb{E} \mathbf{x}\|^2 \\ &= \min_{\boldsymbol{\theta}} \|\mathbf{A}\boldsymbol{\theta} - \mathbf{y}^\delta\|^2 + \text{Trace}(A\Sigma A^T) + \alpha \text{Trace}(\Sigma) + \alpha \|\boldsymbol{\theta}\|^2, \end{aligned}$$

where⁸ the expectation \mathbb{E} is taken with respect to $\mathbf{x} \sim d^{\pi_{\boldsymbol{\theta}}}$. It implies that the following $\boldsymbol{\theta}^*$ is a solution to the minimization problem:

$$\boldsymbol{\theta}^* = (A^T A + \alpha I)^{-1} A^T \mathbf{y}^\delta. \quad (12)$$

Then, the invariant distribution $d^{\pi_{\boldsymbol{\theta}^*}}$ of the Markov chain $\{\mathbf{x}_t\}$ generated by $\pi_{\boldsymbol{\theta}^*}$ is $\mathcal{N}(\boldsymbol{\theta}^*, \Sigma)$. That is, the mean of \mathbf{x}_t 's limiting distribution as $t \rightarrow +\infty$ is $\boldsymbol{\theta}^* = (A^T A + \alpha I)^{-1} A^T \mathbf{y}^\delta$, which is also the Tikhonov regularization solution to the above linear inverse problem. For noise-free data $\mathbf{y}_e = f(\mathbf{x}_e)$, the regularization parameter should be vanishing (i.e. $\alpha = 0$), and the mean of the limiting distribution of \mathbf{x}_t becomes $A^- \mathbf{y}_e$, where A^- denotes the Moore-Penrose inverse of A .

Now, we prove that with $\pi_{\boldsymbol{\theta}}$ defined in (11), the invariant distribution $d^{\pi_{\boldsymbol{\theta}}}$ of $\{\mathbf{x}_t\}$ generated by $\pi_{\boldsymbol{\theta}}$ is the Gaussian distribution $\mathcal{N}(\boldsymbol{\theta}, \Sigma)$. According to knowledge on Markov chains, the invariant distribution $\{d^{\pi_{\boldsymbol{\theta}}}(\mathbf{x})\}_{\mathbf{x} \in \mathcal{S}}$ is a non-negative function satisfying the following two equations

$$\begin{cases} \int_{\mathbf{x} \in \mathcal{S}} d^{\pi_{\boldsymbol{\theta}}}(\mathbf{x}) = 1, \\ d^{\pi_{\boldsymbol{\theta}}}(\mathbf{x}) = \int_{\mathbf{x}' \in \mathcal{S}} d^{\pi_{\boldsymbol{\theta}}}(\mathbf{x}') p^{\pi_{\boldsymbol{\theta}}}(\mathbf{x}|\mathbf{x}'), \quad \text{for any } \mathbf{x} \in \mathcal{S}, \end{cases} \quad (13)$$

⁸We explain the last equality. Denote $\mathbf{z} := A\mathbf{x} - \mathbb{E} A\mathbf{x} \in \mathbb{R}^q$. Then, $\mathbb{E} \|A\mathbf{x} - \mathbb{E} A\mathbf{x}\|^2 = \mathbb{E} [\mathbf{z}^T \mathbf{z}] = \mathbb{E} [\text{Trace}(\mathbf{z}\mathbf{z}^T)] = \text{Trace}(\mathbb{E}[\mathbf{z}\mathbf{z}^T]) = \text{Trace}(A\text{Var}(\mathbf{x})A^T) = \text{Trace}(A\Sigma A^T)$.

where $p^{\pi_{\theta}}(\mathbf{x}|\mathbf{x}')$ denotes the transition probability of the Markov chain $\{\mathbf{x}_t\}$ generated by following π_{θ} . Then,

$$\begin{aligned} d^{\pi_{\theta}}(\mathbf{x}) &= \int_{\mathbf{x}' \in \mathcal{S}} d^{\pi_{\theta}}(\mathbf{x}') p^{\pi_{\theta}}(\mathbf{x}|\mathbf{x}'), \\ &= \int_{\mathbf{x}' \in \mathcal{S}} d^{\pi_{\theta}}(\mathbf{x}') \pi_{\theta}(\mathbf{x} - \mathbf{x}'|\mathbf{x}'), \text{ since } \mathbf{x} = \mathbf{x}' + \mathbf{a}, \\ &= \int_{\mathbf{x}' \in \mathcal{S}} d^{\pi_{\theta}}(\mathbf{x}') \frac{1}{(2\pi)^{n/2} |\det(\Sigma)|^{1/2}} \exp\left(-(\mathbf{x} - \boldsymbol{\theta})^T \Sigma^{-1} (\mathbf{x} - \boldsymbol{\theta})\right), \text{ by (11),} \\ &= \frac{1}{(2\pi)^{n/2} |\det(\Sigma)|^{1/2}} \exp\left(-(\mathbf{x} - \boldsymbol{\theta})^T \Sigma^{-1} (\mathbf{x} - \boldsymbol{\theta})\right), \text{ by (13),} \end{aligned}$$

which implies $d^{\pi_{\theta}} = \mathcal{N}(\boldsymbol{\theta}, \Sigma)$. Here, $|\det(\Sigma)|$ denotes the absolute value of the determinant of Σ .

2.4 Example II: reinforcement learning goal (10) yields iterative regularization

Consider the same linear inverse problem in Section 2.3. We show that when π takes the functional form of (15), the way π_{θ^*} updates $\{\mathbf{x}_t\}$ is equivalent to some well-known algorithms in the field of inverse problems, where $\boldsymbol{\theta}^*$ denotes the solution to (10). In the following, we derive the expression for $d^{\pi_{\theta}}$ and plug it to (10) to obtain the solution $\boldsymbol{\theta}^*$ in (18). Then, in (19) we write the transition rule by π_{θ^*} and show that it is equivalent to the (stochastic) Landweber iteration in certain circumstances.

Define

$$B := \omega(A^T A + \epsilon I), \quad (14)$$

where I represents the identity matrix in $\mathbb{R}^{q \times q}$, $\omega \in (0, \frac{1}{3(\|A\|^2 + \epsilon)})$, and $\|A\|$ denotes the spectral norm of A . Set

$$\pi_{\theta}(\cdot|\mathbf{x}) := \mathcal{N}(\boldsymbol{\theta} - B\mathbf{x}, \sigma^2 I), \quad \text{for any } \mathbf{x} \in \mathcal{S} := \mathbb{R}^q, \quad (15)$$

where $\sigma \geq 0$ is pre-selected and $\boldsymbol{\theta} \in \mathbb{R}^q$. The transition rule in the trajectory generated by π_{θ} is

$$\mathbf{x}_{t+1} = \mathbf{x}_t + \mathbf{a}_t = \boldsymbol{\theta} + (I - B)\mathbf{x}_t + \sigma \mathbf{z}_t,$$

where $\mathbf{z}_t \sim \mathcal{N}(0, I)$ is independent from \mathbf{x}_t . This implies

$$\mathbf{x}_t = \sum_{i=0}^{t-1} (I - B)^i \boldsymbol{\theta} + \sum_{i=0}^{t-1} (I - B)^i \sigma \mathbf{z}_{t-i-1} + (I - B)^t \mathbf{x}_0. \quad (16)$$

This equality and the fact that $\{\mathbf{z}_t\}$ are independent Gaussians imply that \mathbf{x}_t follows $\mathcal{N}(\mu_t, \Sigma_t)$ given that \mathbf{x}_0 is a fixed vector, where

$$\mu_t := \sum_{i=0}^{t-1} (I - B)^i \boldsymbol{\theta} + (I - B)^t \mathbf{x}_0,$$

and

$$\Sigma_t := \sum_{i=0}^{t-1} (I - B)^i \sigma I ((I - B)^i \sigma I)^T = \sigma^2 \sum_{i=0}^{t-1} (I - B)^{2i}.$$

Since $\omega \in (0, \frac{1}{3(\|A\|^2 + \epsilon)})$, we have⁹ $\|I - B\| < 1$. Hence,

$$\lim_{t \rightarrow \infty} \mu_t = B^{-1}\boldsymbol{\theta} \text{ and } \lim_{t \rightarrow \infty} \Sigma_t = \sigma^2(2B - B^2)^{-1}.$$

This implies by Levy's theorem for characteristic functions (e.g., [3, Theorem 26.3]) that the limiting distribution $d^{\pi_{\boldsymbol{\theta}}}$ of \mathbf{x}_t as $t \rightarrow \infty$ is Gaussian with its mean equal to $B^{-1}\boldsymbol{\theta}$ and its variance equal to $\sigma^2(2B - B^2)^{-1}$, namely

$$d^{\pi_{\boldsymbol{\theta}}} = \mathcal{N}(B^{-1}\boldsymbol{\theta}, \sigma^2(2B - B^2)^{-1}). \quad (17)$$

Now, we derive an expression for the solution $\boldsymbol{\theta}^*$ to (10) when $\Omega(\mathbf{x}) = \|\mathbf{x}\|^2$ and $\beta = 0$. Rewrite (10) as:

$$\begin{aligned} \min_{\boldsymbol{\theta}} \mathbb{E}_{\mathbf{x} \sim d^{\pi_{\boldsymbol{\theta}}}} [\|\mathbf{A}\mathbf{x} - \mathbf{y}^{\delta}\|^2 + \alpha\|\mathbf{x}\|^2] \\ &= \min_{\boldsymbol{\theta}} \|\mathbf{A}\mathbb{E}\mathbf{x} - \mathbf{y}^{\delta}\|^2 + \mathbb{E}\|\mathbf{A}\mathbf{x} - \mathbf{A}\mathbb{E}\mathbf{x}\|^2 + \alpha\mathbb{E}\|\mathbf{x} - \mathbb{E}\mathbf{x}\|^2 + \alpha\|\mathbb{E}\mathbf{x}\|^2 \\ &= \min_{\boldsymbol{\theta}} \|\mathbf{A}\mathbb{E}\mathbf{x} - \mathbf{y}^{\delta}\|^2 + \text{Trace}(\mathbf{A}\text{Var}(\mathbf{x})\mathbf{A}^T) + \alpha\text{Trace}(\text{Var}(\mathbf{x})) + \alpha\|\mathbb{E}\mathbf{x}\|^2 \\ &= \min_{\boldsymbol{\theta}} \|\mathbf{A}B^{-1}\boldsymbol{\theta} - \mathbf{y}^{\delta}\|^2 + \sigma^2\text{Trace}(\mathbf{A}(2B - B^2)^{-1}\mathbf{A}^T) \\ &\quad + \alpha\sigma^2\text{Trace}((2B - B^2)^{-1}) + \alpha\|B^{-1}\boldsymbol{\theta}\|^2 \end{aligned}$$

By the first-order necessary condition for optimality, the solution $\boldsymbol{\theta}^*$ is

$$\boldsymbol{\theta}^* = (B^{-1}\mathbf{A}^T\mathbf{A}B^{-1} + \alpha B^{-2})^{-1} B^{-1}\mathbf{A}^T\mathbf{y}^{\delta}, \quad (18)$$

where recall that B is defined in (14).

By (6) and (15), the iteration rule in the trajectory generated by $\pi_{\boldsymbol{\theta}^*}$ is (recall that it means $\mathbf{a}_t \sim \pi_{\boldsymbol{\theta}^*}(\cdot|\mathbf{x}_t)$)

$$\begin{aligned} \mathbf{x}_{t+1} &= \mathbf{x}_t + \mathbf{a}_t = \mathbf{x}_t + \boldsymbol{\theta}^* - B\mathbf{x}_t + \sigma\mathbf{z}_t \\ &= \mathbf{x}_t + (B^{-1}\mathbf{A}^T\mathbf{A}B^{-1} + \alpha B^{-2})^{-1} B^{-1}\mathbf{A}^T\mathbf{y}^{\delta} - B\mathbf{x}_t + \sigma\mathbf{z}_t \\ &= \mathbf{x}_t + \omega(\mathbf{A}^T\mathbf{A} + \epsilon I) [(A^T\mathbf{A} + \alpha I)^{-1}\mathbf{A}^T\mathbf{y}^{\delta} - \mathbf{x}_t] + \sigma\mathbf{z}_t. \end{aligned} \quad (19)$$

where $\mathbf{z}_t \sim \mathcal{N}(0, I)$ and the last equality is by (18). When $\epsilon = \alpha = \sigma = 0$ and $\mathbf{A}^T\mathbf{A}$ is invertible, plugging (14) to above iteration rule gives the conventional Landweber method. That is,

$$\mathbf{x}_{t+1} = \mathbf{x}_t + \omega\mathbf{A}^T(\mathbf{y}^{\delta} - \mathbf{A}\mathbf{x}_t), \quad t = 1, 2, \dots$$

If $\epsilon = \alpha = 0$ and $\sigma \neq 0$, we obtain the stochastic Landweber method [35]:

$$\mathbf{x}_{t+1} = \mathbf{x}_t + \omega\mathbf{A}^T(\mathbf{y}^{\delta} - \mathbf{A}\mathbf{x}_t) + \sigma\mathbf{z}_n, \quad t = 1, 2, \dots$$

When $\epsilon = \alpha \neq 0$ and $\sigma \neq 0$, we derive another simple iteration scheme:

$$\mathbf{x}_{t+1} = (1 - \omega\epsilon)\mathbf{x}_t + \omega\mathbf{A}^T(\mathbf{y}^{\delta} - \mathbf{A}\mathbf{x}_t) + \sigma\mathbf{z}_n, \quad t = 1, 2, \dots$$

3 Main results

Before formulating our main theorem, let us recall the policy gradient theorem and the REINFORCE Algorithm.

⁹ $\|B\| \leq \omega(\|A\|^2 + \epsilon) < 1/3$. Also, by definition B is symmetric and positive definite. Hence, $\|I - B\| < 1$.

3.1 Policy Gradient Theorem

The well-known policy gradient theorem is on the expression of the gradient $\nabla J_T(\boldsymbol{\theta})$. It has different versions and we derive the one for our problem, which can also be found in [37]. Starting from the initial \mathbf{x}_0 with a given distribution, let $h_T := \{(\mathbf{x}_t, \mathbf{a}_t)\}_{t=0}^{T-1}$ denote the trajectory generated following $\pi_{\boldsymbol{\theta}}$, and let \mathcal{H}_T denote the sample space of h_T . Also, define

$$R(h_T) := \frac{1}{T} \sum_{t=0}^{T-1} R(\mathbf{x}_t, \mathbf{a}_t).$$

Then, by the definition of $J_T(\boldsymbol{\theta})$ in (5),

$$\begin{aligned} \nabla J_T(\boldsymbol{\theta}) &= \nabla \mathbb{E}_{h_T \sim \pi_{\boldsymbol{\theta}}} [R(h_T)] = \nabla \left(\sum_{h \in \mathcal{H}_T} p_{\boldsymbol{\theta}}(h_T) R(h_T) \right) = \sum_{h_T \in \mathcal{H}_T} \nabla p_{\boldsymbol{\theta}}(h_T) R(h_T) \\ &= \sum_{h_T \in \mathcal{H}_T} p_{\boldsymbol{\theta}}(h_T) \nabla \ln p_{\boldsymbol{\theta}}(h_T) R(h_T) = \mathbb{E}_{h_T \sim \pi_{\boldsymbol{\theta}}} [\nabla \ln p_{\boldsymbol{\theta}}(h_T) R(h_T)] \\ &= \mathbb{E}_{h_T \sim \pi_{\boldsymbol{\theta}}} \left[R(h_T) \nabla \sum_{t=0}^{T-1} \ln \pi_{\boldsymbol{\theta}}(\mathbf{a}_t | \mathbf{x}_t) \right] = \mathbb{E}_{h_T \sim \pi_{\boldsymbol{\theta}}} \left[R(h_T) \sum_{t=0}^{T-1} \nabla \ln \pi_{\boldsymbol{\theta}}(\mathbf{a}_t | \mathbf{x}_t) \right], \end{aligned}$$

where $p_{\boldsymbol{\theta}}(h_T)$ denotes the probability mass of trajectory h_T following policy $\pi_{\boldsymbol{\theta}}$.

Based on the above expression, a sample estimate of $\nabla J_T(\boldsymbol{\theta})$ is

$$\hat{\nabla} J_T(\boldsymbol{\theta}) := \frac{1}{L} \sum_{l=0}^{L-1} \left[R(h_T^l) \sum_{t=0}^{T-1} \nabla \ln \pi_{\boldsymbol{\theta}}(\mathbf{a}_t^l | \mathbf{x}_t^l) \right], \quad (20)$$

where h_T^l denotes the l^{th} sample of h_T .

3.2 The REINFORCE Algorithm

The REINFORCE is a stochastic gradient ascent algorithm to iteratively improve $J_T(\boldsymbol{\theta})$. The updating term is $\hat{\nabla} J_T(\boldsymbol{\theta})$ in (20). Specifically, given the current value $\boldsymbol{\theta}_n$, we generate L trajectories¹⁰ following $\pi_{\boldsymbol{\theta}_n}$ and update $\boldsymbol{\theta}_n$ according to

$$\boldsymbol{\theta}_{n+1} = \boldsymbol{\theta}_n + a_n (\hat{\nabla} J_T(\boldsymbol{\theta}_n) - 2\beta \boldsymbol{\theta}_n), \quad n \in \mathbb{Z}^+ \cup \{0\}, \quad (21)$$

where $\boldsymbol{\theta}_0 \in \mathbb{R}^d$ is randomly initialized, $\hat{\nabla} J_T(\boldsymbol{\theta})$ is computed according to (20) using the generated L trajectories, $a_n > 0$ is the update step size, and the last term is for regularization purposes. Note that L and T are pre-selected by the user and do not change with n .

3.3 Assumptions and main theorem

In our main theorem, we use the ODE method in stochastic approximation theory to prove that the REINFORCE algorithm asymptotically finds a local optimum of $\boldsymbol{\theta}$ for any pre-selected positive integers L and T . For this purpose we rewrite the updating rule (21) as

$$\boldsymbol{\theta}_{n+1} = \boldsymbol{\theta}_n + a_n (g(\boldsymbol{\theta}_n) + M_{n+1}), \quad n \in \mathbb{Z}^+ \cup \{0\}, \quad (22)$$

where

¹⁰Note that the initial state \mathbf{x}_0 in each trajectory is drawn from a user-specified distribution that is irrelevant to $\pi_{\boldsymbol{\theta}}$, and remain fixed as n increases. One common choice is to set \mathbf{x}_0 as a fixed point.

- $g(\boldsymbol{\theta}_n) := \nabla J_T(\boldsymbol{\theta}_n) - 2\beta\boldsymbol{\theta}_n$.
- $M_{n+1} := \hat{\nabla} J_T(\boldsymbol{\theta}_n) - \nabla J_T(\boldsymbol{\theta}_n)$.

Remark 1. *The convergence analysis for stochastic gradient descent (e.g., Theorem 2 in [7]) does not apply to (22) since the distribution of the error M_n may change with n .*

We state our assumptions needed by our Theorem 1. Assumption 1 and 2 are standard in the convergence analysis of stochastic approximation algorithms (e.g., [4, Section 8.1] and [18, 2, 16]). The boundedness assumption (Assumption 2) is also common for the convergence analysis of algorithms such as stochastic gradient descent.

Assumption 1. 1. $g : \mathbb{R}^d \rightarrow \mathbb{R}^d$ defined as in (22) is Lipschitz: there exists $L_g > 0$ such that for any $\boldsymbol{\theta}, \boldsymbol{\alpha} \in \mathbb{R}^d$ we have

$$\|g(\boldsymbol{\theta}) - g(\boldsymbol{\alpha})\| \leq L_g \|\boldsymbol{\theta} - \boldsymbol{\alpha}\|.$$

2. $\{M_n\}$ are integrable and satisfy for any $n \geq 0$ that

$$\mathbb{E} [\|M_{n+1}\|^2 | \mathcal{F}_n] \leq K(1 + \|\boldsymbol{\theta}_n\|^2),$$

where $K > 0$ is some scalar and \mathcal{F}_n is as defined in Lemma 1.

3. $\{a_n\}$ are positive scalars satisfying

- $\sum_n a_n = +\infty$;
- $\sum_n a_n^2 < +\infty$.

Examples of $\{a_n\}$ satisfying Point 3 in Assumption 1 are: $a_n = \frac{1}{n}, \frac{1}{n \log n}, \dots$.

Assumption 2. Assume that there exists $B_1 > 0$ such that almost surely,

$$\boldsymbol{\theta}_n \in \overline{U(\mathbf{0}; B_1)} := \{\boldsymbol{\theta} \mid \boldsymbol{\theta} \in \mathbb{R}^d, \|\boldsymbol{\theta}\| \leq B_1\}, \text{ for all } n \in \mathbb{Z}^+ \cup \{0\}.$$

Assumption 3. Assume that $\sup_{\boldsymbol{\theta} \in O} \{J_T(\boldsymbol{\theta}) - \alpha\|\boldsymbol{\theta}\|^2\} < +\infty$, and the set of maximum points,

$$H^* := \{\boldsymbol{\theta}^* \in \overline{U(\mathbf{0}; B_1)} \mid \|J_T(\boldsymbol{\theta}^*) - \alpha\|\boldsymbol{\theta}^*\|^2 \geq J_T(\boldsymbol{\theta}) - \alpha\|\boldsymbol{\theta}\|^2 \text{ for any } \boldsymbol{\theta} \in \overline{U(\mathbf{0}; B_1)}\},$$

is non-empty and contains all the critical points of $(J_T(\boldsymbol{\theta}) - \alpha\|\boldsymbol{\theta}\|^2)$ in $\overline{U(\mathbf{0}; B_1)}$.

Assumption 4. Assume that $\overline{U(\mathbf{0}; B_1)}$ as defined in Assumption 2 is an invariant set for the ODE $\dot{\boldsymbol{\theta}}(t) = g(\boldsymbol{\theta}(t))$.

Now we are in the position to present our main theoretical result.

Theorem 1. *Under Assumptions 1-4, the REINFORCE algorithm (22) produces $\boldsymbol{\theta}_n$ that converges almost surely to H^* , the set of maximum points of $J_T(\boldsymbol{\theta}) - \beta\|\boldsymbol{\theta}\|^2$ in $\overline{U(\mathbf{0}; B_1)}$ as defined in A2 with $J_T(\boldsymbol{\theta})$ as defined in (5). That is,*

$$\lim_{n \rightarrow +\infty} \inf_{\boldsymbol{\theta}^* \in H^*} \|\boldsymbol{\theta}_n - \boldsymbol{\theta}^*\| = 0, \quad \text{almost surely (a.s.).} \quad (23)$$

3.4 REINFORCE-IP

Based on the above analysis, we propose an efficient regularization algorithm for non-linear inverse source problem (**IP**), as shown in Algorithms 1 and 2.

Algorithm 1 REINFORCE-IP for solving inverse problems (**IP**).

- 1: Input the forward model f and noisy data $\{\mathbf{y}_k^\delta\}_{k=1}^K$.
 - 2: Train the action rule π_θ according to Algorithm 2.
 - 3: Produce samples of approximate solution $\{\mathbf{x}\}$.
 - 4: Construct the statistics of approximate solution, i.e. the expectation and confidence intervals.
-

Algorithm 2 REINFORCE for constructing the action rule π_θ .

- 1: Design the structure of π_θ .
- 2: Construct the reward function R .
- 3: Define the distribution of the initial state \mathbf{x}_0 .
- 4: Set values of the hyper-parameters $\{\mathcal{N}_\theta, T, H_0, N, L, \alpha, \beta\}$.
- 5: Initialize the weights in \mathcal{N}_θ as θ_0 , and $n = 0$.
- 6: **while** $n < N$ **do**
- 7: Follow π_{θ_n} to generate L length- T trajectories $\{h_l^T\}_{l=0}^{T-1}$.
- 8: Compute $\bar{\mathbf{x}}_t = \frac{1}{L} \sum_{l=0}^{L-1} \mathbf{x}_{l,t}$ for each $t \in \{0, 1, 2, \dots, T-1\}$, where $\mathbf{x}_{l,t}$ is the step- t state in trajectory h_l^T .
- 9: Compute $r = \sum_{t=0}^{T-1} R(\bar{\mathbf{x}}_t, 0)$.
- 10: **if** $r > H_0$ **then**
- 11: break;
- 12: **end if**
- 13: Compute $\hat{\nabla} J_T(\theta)$ according to (20), i.e.

$$\hat{\nabla} J_T(\theta) := \frac{1}{L} \sum_{l=0}^{L-1} \left[R(h_l^T) \sum_{t=0}^{T-1} \nabla \ln \pi_\theta(\mathbf{a}_t^l | \mathbf{x}_t^l) \right],$$

- 14: Follow (21) to update θ_n to get θ_{n+1} , i.e.

$$\theta_{n+1} = \theta_n + a_n (\hat{\nabla} J_T(\theta_n) - 2\beta \theta_n).$$

- 15: **end while**
-

We provide a briefly explanation on each step of Algorithm 2 as follows.

- The structure of the distribution of action π_θ can be designed as a multivariate normal distribution with its mean and covariance equal to the output of a neural network \mathcal{N}_θ whose input is a state \mathbf{x} .
- The functional form of the reward function $R(\cdot, \cdot)$ can be constructed by either (7) or (8), with the expectation is replaced by sample average.
- The initial state \mathbf{x}_0 is used for generating L trajectories $\{h_l^T\}_{l=0}^{L-1}$ in Eq. (20). In practice, the initial state is usually assumed to be a Gaussian or a discrete random variable with some possible approximate solutions of inverse problems.

- The meanings of hyper-parameters are: the architecture of neural network \mathcal{N}_θ , i.e. the number of hidden layers and nodes; the trajectory length T ; the threshold H_0 for the stop-training rule; the prescribed total number of θ -update N ; the number L of trajectories used for one update of θ ; the regularization parameters α and β .
- Note that the larger $R(\mathbf{x}, 0)$ is, the closer $f(\mathbf{x})$ is to $\{\mathbf{y}_k^\delta\}_{k=1}^K$, no matter whether R takes the form of (7) or (8). This is the reason why we use r defined in line 9 of Algorithm 2 as a performance indicator of the policy π_θ .

4 Proof of Theorem 1

4.1 Lemmas

Lemma 1. *Given point 2 in Assumption 1, $\{M_n\}$ defined in (22) is a martingale difference sequences with respect to the increasing σ -fields*

$$\mathcal{F}_n := \sigma(\theta_m, M_m, m \leq n), \quad n \geq 0,$$

where $\sigma(\theta_m, M_m, m \leq n)$ denotes the smallest σ -field that contains $\{\sigma(M_m)\}_{m=0}^n$ and $\{\sigma(\theta_m)\}_{m=0}^n$.

Proof. It suffices to prove that $U_n := \sum_{k=0}^n M_k$ is a martingale with respect to \mathcal{F}_n . First, it is straightforward to see that U_n is integrable under point 2 of Assumption 1. Second, U_n is \mathcal{F}_n -measurable since it is the sum of a finite number of \mathcal{F}_n -measurable mappings (see [19, Theorem 1.91]). Finally,

$$\begin{aligned} \mathbb{E}[U_{n+1}|\mathcal{F}_n] &= \mathbb{E}[M_{n+1}|\mathcal{F}_n] + \mathbb{E}[U_n|\mathcal{F}_n] \\ &= \mathbb{E}[M_{n+1}|\mathcal{F}_n] + U_n \mathbb{E}[\mathbf{1}|\mathcal{F}_n], \text{ since } U_n \text{ is } \mathcal{F}_n\text{-measurable,} \\ &= \mathbb{E}[\hat{\nabla} J_T(\theta_n) - \nabla J_T(\theta_n) | \mathcal{F}_n] + U_n, \quad \text{by the definition of } M_{n+1}, \\ &= \mathbb{E}[\mathbf{0}|\mathcal{F}_n] + U_n, \\ &= U_n. \end{aligned}$$

Therefore, $\{U_n\}$ satisfies the conditions required for being a martingale. Hence, $M_n = U_n - U_{n-1}$ is a martingale difference sequence. \square

Lemma 2. *Under Assumption 1, 2, and 4, for any $\Delta > 0$ we have*

$$\lim_{s \rightarrow +\infty} \left(\sup_{t \in [s, s+\Delta]} \|\bar{\theta}(t) - \theta^s(t)\| \right) = 0, \quad a.s. \quad (24)$$

where

- $\bar{\theta}(\cdot) : [0, +\infty) \rightarrow \mathbb{R}^l$ is the continuous-time linear interpolation for $\{\theta_n\}_{n=0}^\infty$, defined as $\bar{\theta}(t) := \lambda_t \theta_n + (1 - \lambda_t) \theta_{n+1}$ for $t \in [s_n, s_{n+1}]$, where $s_n := \sum_{i=0}^{n-1} a_i$ for any $n > 0$, $s_0 := 0$, and $\lambda_t := \frac{s_{n+1} - t}{s_{n+1} - s_n} \in [0, 1]$.
- $\{\theta_n\}_{n=0}^{+\infty}$ is the sequence produced by the iteration (22) (same as (21)).
- For any $s \geq 0$, $\theta^s(t)$ denotes a solution to the following ODE with $\theta^s(s) = \bar{\theta}(s)$.

$$\dot{\theta}(t) = g(\theta(t)), \quad t \geq s. \quad (25)$$

Remark 2. Note that $\bar{\theta}(t)$ and $\theta^s(t)$ starts from the same point at time $t = s$ and are close to each other only in a finite period $[s, s + \Delta]$. The reason that they are not close to each other in the entire time interval $[s, +\infty)$ is due to the fact that the noise $\{M_n\}_{n=1}^{+\infty}$ is a martingale difference sequence rather than a sequence of i.i.d mean-zero variables.

We define some symbols that are frequently used in the proof.

- For any $t \geq 0$, define

$$[t]^- := \max_{n \geq 0} \{s_n | s_n \leq t\} \text{ and } [t]^+ := \min_{n \geq 0} \{s_n | s_n \geq t\}. \quad (26)$$

- Let m_Δ denote the non-negative integer such

$$s_{n+m_\Delta} := [s_n + \Delta]^-. \quad (27)$$

- $B_g := \sup_{\theta \in \overline{U(\mathbf{0}; B_1)}} \|g(\theta)\| \in [0, +\infty)$.

Proof of Lemma 2. Step 1. We prove that Eq. (24) can be implied by

$$\lim_{n \rightarrow +\infty} \left(\sup_{t \in [s_n, [s_n + \Delta]^-]} \|\bar{\theta}(t) - \theta^{s_n}(t)\| \right) = 0, \quad \text{for any fixed } \Delta > 0. \quad (28)$$

The proof of this implication is given in the Appendix 2.

The following steps prove Eq. (28), and here we make a preview. Step 2-5 prove that for any fixed and sufficiently large integer n we have

$$\sup_{t \in [s_n, s_n + \Delta]} \|\bar{\theta}(t) - \theta^{s_n}(t)\| \leq K_n e^{L_g \Delta} + B_g \sup_{k \geq 0} a_{n+k} \quad (29)$$

where K_n is as defined in Eq. (31). Step 6 proves that $\lim_{n \rightarrow +\infty} K_n = 0$. Also, Point 3 of Assumption 1 implies that $\lim_{n \rightarrow \infty} a_n = 0$, which further implies $\lim_{n \rightarrow +\infty} B_g \sup_{k \geq 0} a_{n+k} = 0$. Therefore, the right-hand side of (29) approaches 0 as $n \rightarrow +\infty$, which further implies (28).

Now, we make explanations on some symbols used in Step 2-6. Note that $\Delta > 0$ is considered fixed. Since $\lim_{n \rightarrow \infty} a_n = 0$, there exists $N_\Delta > 0$ such that whenever $n > N_\Delta$ we have $a_n = s_{n+1} - s_n < \Delta \Rightarrow s_{n+1} < s_n + \Delta$, which further implies $m_\Delta \geq 1$.

Step 2. For any $m \in \mathbb{Z}^+$, we re-write $\bar{\theta}(s_{n+m})$ as follows

$$\bar{\theta}(s_{n+m}) = \bar{\theta}(s_n) + \sum_{k=0}^{m-1} a_{n+k} g(\bar{\theta}(s_{n+k})) + \delta_{n,n+m},$$

where $\delta_{n,n+m} = \sum_{i=0}^{m-1} a_{n+i} M_{n+i+1}$. This equality holds due to $\bar{\theta}(s_k) = \theta_k$ for any non-negative integer k , and the θ -updating algorithm specified in (22).

By the definition of $\theta^{s_n}(\cdot)$ above (25), we re-write $\theta^{s_n}(s_{n+m})$ as

$$\begin{aligned} \theta^{s_n}(s_{n+m}) &= \theta(s_n) + \int_{s_n}^{s_{n+m}} g(\theta^{s_n}(t)) dt \\ &= \bar{\theta}(s_n) + \int_{s_n}^{s_{n+m}} g(\theta^{s_n}(t)) dt, \quad \text{since } \theta(s_n) = \bar{\theta}(s_n), \\ &= \bar{\theta}(s_n) + \sum_{k=0}^{m-1} a_{n+k} g(\theta^{s_n}(s_{n+k})) + \int_{s_n}^{s_{n+m}} [g(\theta^{s_n}(y)) - g(\theta^{s_n}([y]^-))] dy. \end{aligned}$$

Step 3. Take the difference between the two equations in Step 2 and then we prove that for any fixed $n \in \mathbb{Z}^+$,

$$\|\bar{\boldsymbol{\theta}}(s_{n+m}) - \boldsymbol{\theta}^{s_n}(s_{n+m})\| \leq L_g \sum_{i=0}^{m-1} a_{n+i} \|\bar{\boldsymbol{\theta}}(s_{n+i}) - \boldsymbol{\theta}^{s_n}(s_{n+i})\| + K_n, \text{ for all } m \in \mathbb{Z}^+, \quad (30)$$

where

$$K_n := B_g \lambda_g \sum_{k=0}^{\infty} a_{n+k}^2 + \sup_{j \in \mathbb{Z}^+} \|\delta_{n,n+j}\|, \quad (31)$$

and recall that $B_g := \sup_{\boldsymbol{\theta} \in \overline{U(\mathbf{0}; B_1)}} \|g(\boldsymbol{\theta})\| \in [0, +\infty)$. Note that $\sum_{k=0}^{\infty} a_{n+k}^2 < \infty$ due to Point 3 of Assumption 1.

Proof to Eq. (30): Taking the difference between the two equations in Step 2 gives

$$\begin{aligned} \|\bar{\boldsymbol{\theta}}(s_{n+m}) - \boldsymbol{\theta}^{s_n}(s_{n+m})\| &= \left\| \sum_{k=0}^{m-1} a_{n+k} [g(\bar{\boldsymbol{\theta}}(s_{n+k})) - g(\boldsymbol{\theta}^{s_n}(s_{n+k}))] \right. \\ &\quad \left. - \int_{s_n}^{s_{n+m}} [g(\boldsymbol{\theta}^{s_n}(y)) - g(\boldsymbol{\theta}^{s_n}([y]^-))] dy + \delta_{n,n+m} \right\| \\ &\leq L_g \sum_{k=0}^{m-1} a_{n+k} \|\bar{\boldsymbol{\theta}}(s_{n+k}) - \boldsymbol{\theta}^{s_n}(s_{n+k})\| \\ &\quad + \int_{s_n}^{s_{n+m}} \|g(\boldsymbol{\theta}^{s_n}(y)) - g(\boldsymbol{\theta}^{s_n}([y]^-))\| dy + \sup_{j \in \mathbb{Z}^+} \|\delta_{n,n+j}\|, \end{aligned} \quad (32)$$

where the property¹¹ that the norm of an integral is no greater than the integral of the integrand's norm is used to derive the inequality. Now, we bound the second term in the

¹¹The property is, for any integrable function $f : \mathbb{R} \rightarrow \mathbb{R}^l$ and any $a < b$, we have $\|\int_a^b h(t) dt\| \leq \int_a^b \|h(t)\| dt$. As for the proof, define $v := \int_a^b h(t) dt$. Then,

$$\|v\|^2 = v^T v = \int_a^b v^T h(t) dt \leq \int_a^b \|v\| \cdot \|h(t)\| dt.$$

Dividing both the left-end and the right-end by $\|v\|$ gives the desired inequality.

above,

$$\begin{aligned}
\int_{s_n}^{s_{n+m}} \|g(\boldsymbol{\theta}^{s_n}(y)) - g(\boldsymbol{\theta}^{s_n}([y]^-))\| dy &= \sum_{k=0}^{m-1} \int_{s_{n+k}}^{s_{n+k+1}} \|g(\boldsymbol{\theta}^{s_n}(y)) - g(\boldsymbol{\theta}^{s_n}([y]^-))\| dy \\
&= \sum_{k=0}^{m-1} \int_{s_{n+k}}^{s_{n+k+1}} \|g(\boldsymbol{\theta}^{s_n}(y)) - g(\boldsymbol{\theta}^{s_n}(s_{n+k}))\| dy \\
&\leq \sum_{k=0}^{m-1} \int_{s_{n+k}}^{s_{n+k+1}} \lambda_g \|\boldsymbol{\theta}^{s_n}(y) - \boldsymbol{\theta}^{s_n}(s_{n+k})\| dy \\
&\leq \sum_{k=0}^{m-1} \int_{s_{n+k}}^{s_{n+k+1}} \lambda_g \|g(\boldsymbol{\theta}^{s_n}(\tau_y))(y - s_{n+k})\| dy, \text{ by MVT,} \\
&\leq \lambda_g B_g \sum_{k=0}^{m-1} \int_{s_{n+k}}^{s_{n+k+1}} (y - [y]^-) dy \\
&\leq \lambda_g B_g \sum_{k=0}^{m-1} \int_{s_{n+k}}^{s_{n+k+1}} (s_{n+k+1} - s_{n+k}) dy \\
&\leq \lambda_g B_g \sum_{k=0}^{m-1} a_{n+k}^2,
\end{aligned}$$

where the inequality in the third line is by the mean value theorem (MVT), and the inequality in the fourth line holds since $\|\boldsymbol{\theta}^{s_n}(\tau_y)\| \leq B_1$ (because $\overline{U(\mathbf{0}; B_1)}$ is an invariant set for the ODE $\dot{\boldsymbol{\theta}}(t) = g(x(t))$ by Assumption 4, $\tau_y \geq s_n$, and $\boldsymbol{\theta}^{s_n}(s_n) = \boldsymbol{\theta}_n \in \overline{U(\mathbf{0}; B_1)}$). This finishes proving Eq. (30).

Step 4. By the discrete Gronwall inequality (see Lemma 4 in Appendix 1), Eq. (30) implies for any fixed $n \in \mathbb{Z}^+$,

$$\|\bar{\boldsymbol{\theta}}(s_{n+m}) - \boldsymbol{\theta}^{s_n}(s_{n+m})\| \leq K_n e^{L_g \sum_{i=0}^{m-1} a_{n+i}},$$

holds for all $m \in \mathbb{Z}^+$. Therefore, for any $m \in \{0, 1, \dots, m_\Delta\}$ (where m_Δ is defined in (27) and $m_\Delta \geq 1$ due to the discussion in the last paragraph in Step 1) we have

$$\|\bar{\boldsymbol{\theta}}(s_{n+m}) - \boldsymbol{\theta}^{s_n}(s_{n+m})\| \leq K_n e^{L_g \Delta}, \quad (33)$$

which holds because¹² for $m \in [1, m_\Delta]$:

$$\sum_{i=0}^{m-1} a_{n+i} \leq \sum_{i=0}^{m_\Delta-1} a_{n+i} = s_{n+m_\Delta} - s_n = [s_n + \Delta]^- - s_n \leq \Delta.$$

Step 5. Now, we use Eq. (33) to bound $\|\boldsymbol{\theta}^{s_n}(t) - \bar{\boldsymbol{\theta}}(t)\|$ for any $t \in [s_{n+m}, s_{n+m+1}]$,

¹²Eq.(33) holds trivially for $m = 0$

where m is any integer in $[0, m_\Delta - 1]$. (Recall that $\|\boldsymbol{\theta}^{s_n}(t) - \bar{\boldsymbol{\theta}}(t)\|$ appears in (29).)

$$\begin{aligned}
\|\boldsymbol{\theta}^{s_n}(t) - \bar{\boldsymbol{\theta}}(t)\| &= \|\boldsymbol{\theta}^{s_n}(t) - (\lambda_t \boldsymbol{\theta}_{n+m} + (1 - \lambda_t)(\boldsymbol{\theta}_{n+m+1}))\| \\
&= \|\lambda_t(\boldsymbol{\theta}^{s_n}(t) - \boldsymbol{\theta}_{n+m}) + (1 - \lambda_t)(\boldsymbol{\theta}^{s_n}(t) - \boldsymbol{\theta}_{n+m+1})\| \\
&= \|\lambda_t(\boldsymbol{\theta}^{s_n}(t) - \bar{\boldsymbol{\theta}}(s_{n+m})) + (1 - \lambda_t)(\boldsymbol{\theta}^{s_n}(t) - \bar{\boldsymbol{\theta}}(s_{n+m+1}))\| \\
&= \|\lambda_t \left(\boldsymbol{\theta}^{s_n}(s_{n+m}) - \bar{\boldsymbol{\theta}}(s_{n+m}) + \int_{s_{n+m}}^t g(\boldsymbol{\theta}^{s_n}(s)) ds \right) \\
&\quad + (1 - \lambda_t) \left(\boldsymbol{\theta}^{s_n}(s_{n+m+1}) - \bar{\boldsymbol{\theta}}(s_{n+m+1}) - \int_t^{s_{n+m+1}} g(\boldsymbol{\theta}^{s_n}(s)) ds \right)\| \\
&\leq K_n e^{L_g \Delta} + \int_{s_{n+m}}^{s_{n+m+1}} \|g(\boldsymbol{\theta}^{s_n}(s))\| ds, \quad \text{by (33) and } \lambda_t \in [0, 1], \\
&\leq K_n e^{L_g \Delta} + B_g a_{n+m},
\end{aligned}$$

where recall that $B_g := \sup_{\boldsymbol{\theta} \in \overline{U(0; B_1)}} \|g(\boldsymbol{\theta})\| \in [0, +\infty)$. Therefore, for any $t \in [s_n, s_{n+m_\Delta}] = [s_n, [s_n + \Delta]^-]$, we have

$$\|\boldsymbol{\theta}^{s_n}(t) - \bar{\boldsymbol{\theta}}(t)\| \leq K_n e^{L_g \Delta} + B_g \sup_{m \in \mathbb{Z}^+ \cup \{0\}} a_{n+m},$$

which further implies

$$\sup_{t \in [s_n, [s_n + \Delta]^-]} \|\boldsymbol{\theta}^{s_n}(t) - \bar{\boldsymbol{\theta}}(t)\| \leq K_n e^{L_g \Delta} + B_g \sup_{m \in \mathbb{Z}^+ \cup \{0\}} a_{n+m}. \quad (34)$$

Step 6. Taking the limit on both sides of (34) gives

$$\lim_{n \rightarrow +\infty} \sup_{t \in [s_n, [s_n + \Delta]^-]} \|\boldsymbol{\theta}^{s_n}(t) - \bar{\boldsymbol{\theta}}(t)\| \leq \lim_{n \rightarrow +\infty} [K_n e^{L_g \Delta} + B_g \sup_{m \in \mathbb{Z}^+ \cup \{0\}} a(n+m)] = 0, \quad (35)$$

where the last equality is due to $\lim_{n \rightarrow +\infty} \sup_{m \in \mathbb{Z}^+ \cup \{0\}} a(n+m) = 0$ by Point 3 in Assumption 1 and $\lim_{n \rightarrow +\infty} K_n = 0, a.s.$. The proof for the second limit is given below.

Recall that

$$K_n = B_g \lambda_g \sum_{k=0}^{\infty} a_{n+k}^2 + \sup_{j \in \mathbb{Z}^+} \|\delta_{n,n+j}\|,$$

where recall that

- $B_g < +\infty$ is the upper bound of $\|g(\cdot)\|$ in the region $\{x | x \in \mathbb{R}^d, \|x_n\| \leq B_1\}$ and λ_g is the Lipschitz constant.
- $\sum_{k \geq 0} a_{n+k}^2 \rightarrow 0$ as $n \rightarrow \infty$ by Point 3 of Assumption 1.
- $\delta_{n,n+j} = \sum_{i=0}^{j-1} a_{n+i} M_{n+i+1}$.

Hence, $\lim_{n \rightarrow \infty} B_g \lambda_g \sum_{k=0}^{\infty} a_{n+k}^2 = 0$. Now, it remains to prove that

$$\lim_{n \rightarrow \infty} \sup_{j \in \mathbb{Z}^+} \|\delta_{n,n+j}\| = 0, a.s..$$

Define $\zeta_n := \sum_{i=0}^{n-1} a_i M_{i+1}, n \geq 0$. Then, ζ_n is a martingale with the proof similar to that for Lemma 1. By Point 2 of Assumption 1, for any non-negative integer n we have

$$\begin{aligned}
\mathbb{E}[\|\zeta_{n+1} - \zeta_n\|^2 | \mathcal{F}_n] &= \mathbb{E}[a_n^2 \|M_{n+1}\|^2 | \mathcal{F}_n] \\
&\leq a_n^2 K(1 + \|\boldsymbol{\theta}_n\|^2) \\
&\leq a_n^2 K(1 + B_1^2).
\end{aligned}$$

Therefore, by Lemma 5 (see Appendix 1) $\{\zeta_n\}$ converges almost surely, which implies by Cauchy criterion that

$$\lim_{n \rightarrow +\infty} (\sup_{m \in \mathbb{Z}^+} \|\delta_{n,n+m}\|) = \lim_{n \rightarrow +\infty} (\sup_{m \in \mathbb{Z}^+} \|\zeta_{n+m} - \zeta_n\|) = 0, \text{ a.s.}$$

This finishes the proof to Step 6 and hence the proof to Lemma 2. \square

4.2 Prove Theorem 1

Define $F(\boldsymbol{\theta}) := -J_T(\boldsymbol{\theta}) + \beta\|\boldsymbol{\theta}\|^2$ and $\mu := \inf_{\|\boldsymbol{\theta}\| \leq B_1} F(\boldsymbol{\theta})$. Then, $\nabla J_T(\boldsymbol{\theta}) = -g(\boldsymbol{\theta})$. By Point 1 of Assumption 1, $J_T(\boldsymbol{\theta})$ is continuously differentiable, which implies that $F(\boldsymbol{\theta})$ attains both the maximum and minimum on the closed and bounded set $\overline{U(\mathbf{0}; B_1)}$. Hence, $\mu > -\infty$ and $\emptyset \neq \{\boldsymbol{\theta} \in \overline{U(\mathbf{0}; B_1)} \mid F(\boldsymbol{\theta}) = \mu\} = H^*$ by Assumption 3.

We state an inequality whose proof is given later: For any $\varepsilon > 0$ there exists $T_\varepsilon > 0$ such that whenever $t > T_\varepsilon$ we have

$$F(\bar{\boldsymbol{\theta}}(t)) \leq \mu + (B_g + 1)\varepsilon. \quad (36)$$

Using (36), we prove that for any sequence $\{\tau_n\}_{n=1}^{+\infty}$ such that $\lim_{n \rightarrow +\infty} \tau_n = +\infty$ and $\{\bar{\boldsymbol{\theta}}(\tau_n)\}_{n=0}^\infty$ converges, we have

$$\Theta^* := \lim_{n \rightarrow +\infty} \bar{\boldsymbol{\theta}}(\tau_n) \in H^*. \quad (37)$$

Specifically, for any $\varepsilon > 0$, suppose whenever $n > N_\varepsilon$ we have $\|\bar{\boldsymbol{\theta}}(\tau_n) - \Theta^*\| < \varepsilon$. Then, whenever $n > N_\varepsilon$ and $\tau_n > T_\varepsilon$ hold at the same time, we have

$$\begin{aligned} F(\Theta^*) &= F(\Theta^*) - F(\bar{\boldsymbol{\theta}}(\tau_n)) + F(\bar{\boldsymbol{\theta}}(\tau_n)) \\ &\leq B_g \|\Theta^* - \bar{\boldsymbol{\theta}}(\tau_n)\| + F(\bar{\boldsymbol{\theta}}(\tau_n)), \quad \text{by MVT,} \\ &\leq B_g \|\Theta^* - \bar{\boldsymbol{\theta}}(\tau_n)\| + \mu + (B_g + 1)\varepsilon, \quad \text{by (36),} \\ &< \mu + (2B_g + 1)\varepsilon. \end{aligned}$$

Since $\varepsilon > 0$ can be arbitrarily small, the above inequality implies that $F(\Theta^*) \leq \mu$, which further implies (by the definition of μ) that $F(\Theta^*) = \mu$. Hence, $\Theta^* \in H^*$.

Then, we prove Eq. (23) by contradiction. Assume that Eq. (23) is false. Then, there exists $\varepsilon_0 > 0$ and an increasing sequence $\{s_n\}_{n=0}^\infty \subset \mathbb{R}$ such that $\lim_{n \rightarrow +\infty} s_n = +\infty$ and $\inf_{\boldsymbol{\theta} \in H^*} \|\bar{\boldsymbol{\theta}}(s_n) - \boldsymbol{\theta}\| > \varepsilon_0$. This implies that any limit point y^* of the set $\{\bar{\boldsymbol{\theta}}(s_n)\}_{n=0}^\infty$, which exists since $\{\bar{\boldsymbol{\theta}}(s_n)\}_{n=0}^\infty$ is bounded¹³, satisfies $\inf_{\boldsymbol{\theta} \in H^*} \|y^* - \boldsymbol{\theta}\| > 0$. Therefore, $y^* \notin H^*$, which contradicts the previously derived result of (37). Hence, Eq. (23) holds and Theorem 1 is proved. Now, it remains to prove (36).

4.2.1 Proof to Eq. (36)

For any $\varepsilon > 0$, define $T_\varepsilon := 1 + C/\Delta_\varepsilon + S_\varepsilon$, where

- $\Delta_\varepsilon := \inf_{\boldsymbol{\theta} \in O_\varepsilon} \|g(\boldsymbol{\theta})\|^2$, where $O_\varepsilon := \{\boldsymbol{\theta} \in \overline{U(\mathbf{0}; B-1)} \mid F(\boldsymbol{\theta}) \geq \mu + \varepsilon\}$. Then, $\Delta_\varepsilon > 0$ because (1) O_ε is bounded and closed¹⁴; (2) $\|g(\boldsymbol{\theta})\|^2$ is continuous since $g(\boldsymbol{\theta})$ is Lipschitz, and (3) $\|g(\boldsymbol{\theta})\|^2$ is positive on O_ε since $O_\varepsilon \cap H^* = \emptyset$ ¹⁵ and by Assumption 3 H^* contains all the critical points of F in $\overline{U(\mathbf{0}; B-1)}$.

¹³By Assumption 2, $\{\bar{x}(t)\}_{t \geq 0} \in \overline{U(\mathbf{0}; B_1)}$.

¹⁴This set O_ε is closed because any limit point Θ^* of this set belongs to the closed set $\overline{U(\mathbf{0}; B-1)}$ and satisfies $F(\Theta^*) \geq \mu + \varepsilon$ by the continuity of F , which implies that $\Theta^* \in O_\varepsilon$.

¹⁵Recall that we proved in Section 4.2 that $H^* = \{\boldsymbol{\theta} \in \overline{U(\mathbf{0}; B_1)} \mid F(\boldsymbol{\theta}) = \mu\}$.

- $C := \sup_{\boldsymbol{\theta} \in \overline{U(\mathbf{0}; B_1)}} (F(\boldsymbol{\theta}) - \mu)$.
- $S_\varepsilon > 0$ denotes the threshold such that whenever $s \geq S_\varepsilon$ the following inequality holds

$$\sup_{t \in [s, s+C/\Delta_\varepsilon+1]} \|\bar{\boldsymbol{\theta}}(t) - \boldsymbol{\theta}^s(t)\| \leq \varepsilon, \quad a.s.$$

Note that almost surely S_ε exists due to (24).

Whenever $t > T_\varepsilon$, define $s := t - C/\Delta_\varepsilon - 1$.

$$\begin{aligned}
F(\bar{\boldsymbol{\theta}}(t)) &= F(\bar{\boldsymbol{\theta}}(t)) - F(\boldsymbol{\theta}^s(t)) + F(\boldsymbol{\theta}^s(t)), \\
&\leq |F(\bar{\boldsymbol{\theta}}(t)) - F(\boldsymbol{\theta}^s(t))| + F(\boldsymbol{\theta}^s(t)) \\
&\leq B_g \|\bar{\boldsymbol{\theta}}(t) - \boldsymbol{\theta}^s(t)\| + F(\boldsymbol{\theta}^s(t)), \quad \text{by MVT.} \\
&\leq B_g \|\bar{\boldsymbol{\theta}}(t) - \boldsymbol{\theta}^s(t)\| + \mu + \varepsilon, \quad \text{It will be justified later.} \tag{A} \\
&= B_g \|\bar{\boldsymbol{\theta}}(s + C/\Delta_\varepsilon + 1) - \boldsymbol{\theta}^s(s + C/\Delta_\varepsilon + 1)\| + \mu + \varepsilon, \quad \text{by definition of } s. \\
&\leq B_g \sup_{\tau \in [s, s+C/\Delta_\varepsilon+1]} \|\bar{\boldsymbol{\theta}}(\tau) - \boldsymbol{\theta}^s(\tau)\| + \mu + \varepsilon, \\
&\leq B_g \varepsilon + \mu + \varepsilon, \quad \text{since } s = t - C/\Delta_\varepsilon - 1 > T_\varepsilon - C/\Delta_\varepsilon - 1 = S_\varepsilon, \\
&= \mu + (B_g + 1)\varepsilon.
\end{aligned}$$

This is (36). The final step is to justify (A), which is given below.

We prove the inequality $F(\boldsymbol{\theta}^s(t)) \leq \mu + \varepsilon$ in (A) by contradiction. Assume that $F(\boldsymbol{\theta}^s(t)) > \mu + \varepsilon$. Then, it implies the following inequality for any $u \in [s, t]$

$$F(\boldsymbol{\theta}^s(u)) \geq F(\boldsymbol{\theta}^s(t)) \geq \mu + \varepsilon,$$

which is due to $\frac{dF(\boldsymbol{\theta}^s(u))}{du} = -\|g(\boldsymbol{\theta}^s(u))\|^2 \leq 0$ since by definition $\dot{\boldsymbol{\theta}}^s(u) = g(\boldsymbol{\theta}^s(u))$ for any $u \geq s$. The above inequality implies that for any $u \in [s, t]$,

$$\boldsymbol{\theta}^s(u) \in O_\varepsilon \Rightarrow \|g(\boldsymbol{\theta}^s(u))\|^2 \geq \Delta_\varepsilon.$$

Hence,

$$\begin{aligned}
F(\boldsymbol{\theta}^s(t)) - F(\boldsymbol{\theta}^s(s)) &= \int_s^t dF(x(u)) \\
&= \int_s^t \dot{\boldsymbol{\theta}}^{s\top}(u) g(\boldsymbol{\theta}^s(u)) ds, \quad \text{T denotes matrix transpose.} \\
&= \int_s^t -g^\top(\boldsymbol{\theta}^s(u)) g(\boldsymbol{\theta}^s(u)) du \\
&= - \int_s^t \|g(\boldsymbol{\theta}^s(u))\|^2 ds \\
&\leq -\Delta_\varepsilon(t - s) \\
&< -C, \quad \text{by definition of } s.
\end{aligned}$$

In sum,

$$F(\boldsymbol{\theta}^s(t)) < F(\boldsymbol{\theta}^s(s)) - C = F(\boldsymbol{\theta}^s(s)) + \inf_{\boldsymbol{\theta} \in \overline{U(\mathbf{0}; B_1)}} (\mu - F(\boldsymbol{\theta})) \leq \mu,$$

which is a contradiction, since $F(\boldsymbol{\theta}) \geq \mu$ for all $\boldsymbol{\theta} \in \overline{U(\mathbf{0}; B_1)}$ and $\boldsymbol{\theta}^s(t) \in \overline{U(\mathbf{0}; B_1)}$ due to Assumption 4. This finishes the justification for (A), the proof for Eq. (36), and the proof for Theorem 1.

5 Numerical Experiments

In this section, we apply REINFORCE-IP (i.e. Algorithm 1) to solve two typical non-linear inverse problems. In these two examples, we assume that a set of noised signals $\{\mathbf{y}_k^\delta\}_{k=1}^K$ in (1) are observed. So as a modification of (8) for using all the available data, we set the reward function as

$$R(\mathbf{x}, \mathbf{a}) := \frac{1}{\frac{1}{K} \sum_{k=1}^K \|f(\mathbf{x} + \mathbf{a}) - \mathbf{y}_k^\delta\|^2 + 0.001 + \alpha\Omega(\mathbf{x})}, \quad (38)$$

where $\{\mathbf{y}_k^\delta\}_{k=1}^K$ denote L observed samples of \mathbf{y}^δ in (1). An alternative way to define the reward function is to set it as negative of the denominator (or equivalently $R(\mathbf{x}, \mathbf{a}) = -\frac{1}{K} \sum_{k=1}^K (f(\mathbf{x} + \mathbf{a}) - \mathbf{y}_k^\delta)^2 - \alpha\Omega(\mathbf{x})$). But through experiments we find that the denominator format of R in Eq. (38) works better. As for the functional form of the policy, we set $\pi_\theta(\cdot|\mathbf{x})$ as a multivariate normal distribution with its mean and covariance equal to the output of a neural network \mathcal{N}_θ with input \mathbf{x} and weights θ .

5.1 Auto-convolution equation

In the first group of numerical simulations, we consider the following 1D auto-convolution equation, which has many applications in spectroscopy (e.g. the modern methods of ultrashort laser pulse characterization) [1, 12], the structure of solid surfaces [8] and the nano-structures [11], etc.

$$\int_0^t x(t-s)x(s) ds = y(t). \quad (39)$$

We remark that to the best of our knowledge, results on the existence of $x(t)$ given $y(t)$ for the nonlinear integral equation (39) are quite limited. Hence, to avoid the possibility that there does not exist any $x(t)$ corresponding to a randomly chosen $y(t)$, for our experiment we pre-define

$$x(t) = 10t(1-t)^2, \quad (40)$$

and let $y(t)$ be the corresponding right-hand side in (39).

We test the ability of REINFORCE-IP to numerically solve a discretized version of (39) given noised $y(t)$. Let f be the map from $\mathbf{x} = [x(0), x(\frac{1}{D-1}), x(\frac{2}{D-1}), \dots, x(1)] \in \mathbf{R}^D$, the discretization of $\{x(t)\}_{t \in [0,1]}$, to $\mathbf{y} = [y_0, y_1, \dots, y_{D-1}] \in \mathbb{R}^D$, a discrete-time approximation to $\{y(t)\}_{t \in [0,1]}$, where $(x(t), y(t))$ satisfy Eq. (39). Here, $D \in \mathbb{Z}^+$ denotes the number of discrete points and we set it as $D = 64$ in the experiment. The approximation $\mathbf{y} = f(\mathbf{x})$ is computed in the following way¹⁶: $y_0 = 0$ and for any $j \in \{1, 2, \dots, D-1\}$,

$$y_j = \frac{1}{D-1} \sum_{i=1}^j \frac{1}{2} (x(t_j - t_i)x(t_i) + x(t_j - t_{i-1})x(t_{i-1})),$$

where $t_j := j/(D-1)$.

The inverse problem we will use REINFORCE-IP to solve is

$$f(\mathbf{x}) + \epsilon = \mathbf{y}^\delta, \quad (41)$$

¹⁶By Eq. (39), for any $j \in \{1, 2, \dots, D-1\}$

$$y(t_j) = \sum_{i=1}^j \int_{t_{i-1}}^{t_i} x(t_j - s)x(s)ds \approx \frac{1}{N-1} \sum_{i=1}^j \frac{1}{2} (x(t_j - t_i)x(t_i) + x(t_j - t_{i-1})x(t_{i-1})) = y_j.$$

where $\mathbf{y}^\delta = f(\mathbf{x}_e) + \boldsymbol{\epsilon}$, $\boldsymbol{\epsilon}$ is a mean-zero Gaussian noise, and

$$\mathbf{x}_e = [x(0), x(\frac{1}{N-1}), x(\frac{2}{N-1}), \dots, x(1)] \in \mathbb{R}^D \quad (42)$$

with $x(t)$ defined in Eq. (40) with $D = 64$. This inverse problem has a unique solution \mathbf{x}_e in $U^+ := \{\mathbf{x} \in \mathbb{R}^D : \mathbf{x} \text{ has non-negative entries}\}$, as implied by the following theorem on (39), which further implies there are in total two solutions to (41) in \mathbb{R}^D , \mathbf{x}_e and $-\mathbf{x}_e$.

Theorem 2. (i) (Weak uniqueness [12]) For $y \in L^2[0, 2]$, the integral equation has at most two different solutions $x_1(t), x_2(t) \in L^1[0, 1]$. Moreover, it holds that $x_1(t) + x_2(t) = 0, t \in [0, 1]$.

(ii) (Uniqueness [13]) Define

$$\begin{aligned} S^+ &:= \{x \in L^1[0, 1] : x(t) \geq 0\}, \\ S_\epsilon^+ &:= \{x \in L^1[0, 1] : \epsilon = \sup\{s : x(t) = 0, \text{ a.e. in } [0, s]\}\}, \\ Y_\epsilon^+ &:= \{y \in L^2[0, 2] : \epsilon = \sup\{s : y(t) = 0, \text{ a.e. in } [0, s]\}\}. \end{aligned}$$

Then for $y \in Y_0^+$, the equation (39) has at most one solution in S^+ . Moreover, the solution belongs to S_0^+ .

Next, we state some common assumptions and settings for the REINFORCE-IP algorithm applied in all our later experiments to solve (41). Assume that instead of the exact signal $f(\mathbf{x}_e)$, a set $\{\mathbf{y}_k^\delta\}_{k=1}^{100}$ of noised observations of the right-hand side in (41) are available, which are generated according to $\mathbf{y}_k^\delta := f(\mathbf{x}_e) + \boldsymbol{\epsilon}_k$ where $\boldsymbol{\epsilon}_k$ is a vector of independent mean-zero normal random variables with standard deviations equal to $5\% \mathbf{y}_e$ and $\{\boldsymbol{\epsilon}_k\}_{k=1}^{100}$ are i.i.d. noises.

We construct the policy $\pi_\theta(\cdot|\mathbf{x})$, a distribution over the action space determined by the given state \mathbf{x} , as a multivariate normal distribution whose mean and standard deviation are transformed output¹⁷ from a feed-forward neural network \mathcal{N}_θ with input \mathbf{x} .

As a common practice in the literature of solving (41), assume that we are given the information that the first and last entry in the solution \mathbf{x}_e are all zero. To use this information, we set the regularizer in (38) as

$$\Omega(\mathbf{x}) = |x_0| + |x_{D-1}|.$$

5.1.1 Simulation one

Suppose we are given the additional information that there is a solution to (41) in U^+ . To use it, we let the initial state in any trajectory generated by π_θ be a fixed point in U^+ , which is randomly chosen as $\mathbf{x}_0 = [0.01, 0.01, \dots, 0.01] \in \mathbb{R}^{64}$. This setting increases the likelihood for the RL algorithm to find the solution \mathbf{x}_e in U^+ , since \mathbf{x}_0 is closer to the solution in U^+ (and hence easier to be found by the agent π_θ) than any point not in U^+ . The experiment result shows this setting is effective since all the solution estimates are approximations of $\mathbf{x}_e \in U^+$ (see Figure 4).

We follow the REINFORCE algorithm stated in Section 3.2 to repeatedly update $\boldsymbol{\theta}$, until the sum of rewards¹⁸ in a trajectory generated by the policy exceeds a threshold H_0

¹⁷Let $[\mathbf{z}_1, \mathbf{z}_2]$ of the neural network $\mathcal{N}_\theta(\mathbf{x})$. Then, we let the moving average of \mathbf{z}_1 with a window length of 3 to serve as the mean of π_θ and $\log(1 + e^{\mathbf{z}_2})$ serve as the standard deviation. The moving average is used to ensure the smoothness of the predictions of \mathbf{x}_e . The function $\log(1 + e^{\mathbf{z}_2})$ is called softplus and is a typical method to force outputs from a neural net to be positive.

¹⁸Specifically, after every 100 updates of $\boldsymbol{\theta}$, we use π_θ to generate $L = 1,000$ trajectories $\{\mathbf{x}_{l,t}\}_{t=0}^{T-1}$ for $l \in \{0, 2, \dots, L-1\}$, take the mean of each step to get $\{\bar{\mathbf{x}}_t\}_{t=0}^{T-1}$, and compute the sum $\sum_{t=0}^{T-1} R(\bar{\mathbf{x}}_t, \mathbf{0})$. This sum is considered as the performance of π_θ .

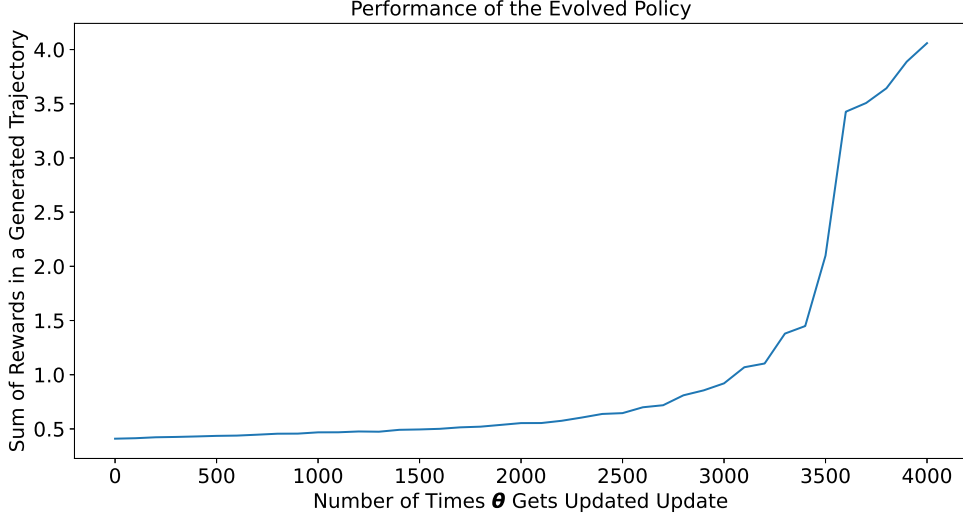


Figure 3: Performance of the Evolving Policy for Simulation One. After every 100 updates of θ -update we calculate the performance of π_θ . For model hyper-parameters, we set $T = 10$, $\alpha = 0.1$, $\beta = 0.125$, $H_0 = 4.0$ (the performance threshold for stopping training). The hidden layers of \mathcal{N}_θ are (64, 64, 64) with the activation function as ReLU. The learning rate is set as $a_n := \frac{0.001}{50,000+n}$.

or the total number of θ -updates exceeds 8,000, which one comes first. Intuitively, this process keeps decreasing the denominator in Eq. (38).

The value of the stop-training-threshold H_0 , T (the number of total time steps taken in a trajectory), α , β (recall (4)), and hyper-parameters of the neural net \mathcal{N}_θ are all selected through cross validation. The selected values are reported below Figure 3, which plots the performance of π_θ during the training process.

Now, we investigate the ability of the trained policy π_θ to find the solution to (41). With π_θ , we generate $L = 10,000$ trajectories of length $T = 10$ and record the last state \mathbf{x}_{T-1} in each trajectory (so that we have $\{\mathbf{x}_{l,T-1}\}_{l=1}^N$ and each $\mathbf{x}_{l,T-1}$ can be viewed as an estimated solution). The R^2 between \mathbf{x}_e and the average $\bar{\mathbf{x}}_{T-1}$ of the N estimate is 85.3%, indicating that π_θ is a successful policy for searching for a solution to the inverse problem. Their graphs, as well as the corresponding forward signals $f(\mathbf{x}_e)$ and $f(\hat{\mathbf{x}}_{T-1})$, are plotted in Figure 4. The shaded region bounded by the two green dashed curves is the estimated 99%-confidence interval obtained by the method of bootstrapping¹⁹ (e.g., [26]). That is, we estimate that for each entry $i \in \{1, 2, \dots, D\}$ this shaded region contains the i^{th} entry of the true solution \mathbf{x}_e with a probability of 99%.

5.1.2 Simulation two

In our second group of simulations, we aim to find only one solution (any one of two solutions) to the inverse problem (41) without the a priori information of solutions. Hence, as a common practice in iterative algorithms, we fix the initial state \mathbf{x}_0 at the origin $\mathbf{0} \in \mathbb{R}^D$.

The procedures for training and testing π_θ are identical to those in simulation one. The history of π_θ 's performance in the θ -updating process is reported in Figure 5 and the solution estimates by the trained model π_θ are plotted in Figure 6. The R^2 statistics between $-\mathbf{x}_e$ and the estimates average $\bar{\mathbf{x}}_{T-1}$ is 86.7%, indicating the RL algorithm's success for finding a solution to (41).

¹⁹Specifically, we bootstrap from the estimates $\{\mathbf{x}_{l,T-1}\}_{l=1}^{1,000}$ for $B = 10,000$ times, compute the mean of each bootstrap copy, and obtain the 0.5%-percentile and 99.5%-percentile of these 10,000 means as the lower and upper bound for the estimated 99%-confidence interval.

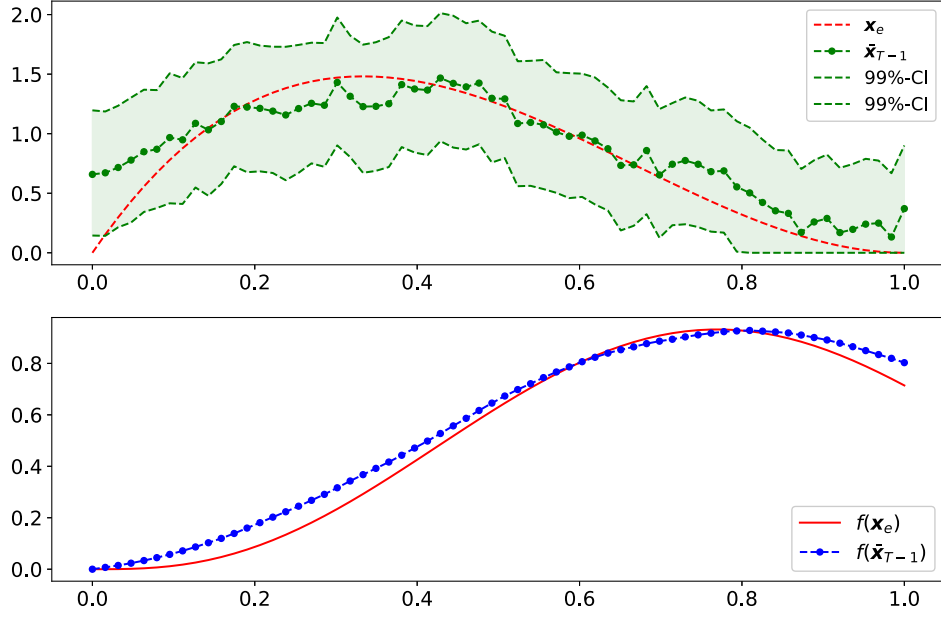


Figure 4: The Estimations and True Values for Simulation One. $\bar{\mathbf{x}}_{T-1}$ is the mean of 10,000 solution estimates, and the region bounded by the two dashed curve of 99%-CI is the confidence interval of the solution estimate obtained by bootstrapping. Since we are looking for a solution in U^+ , negative entries in the lower bound of the 99%-CI are replaced with zeros.

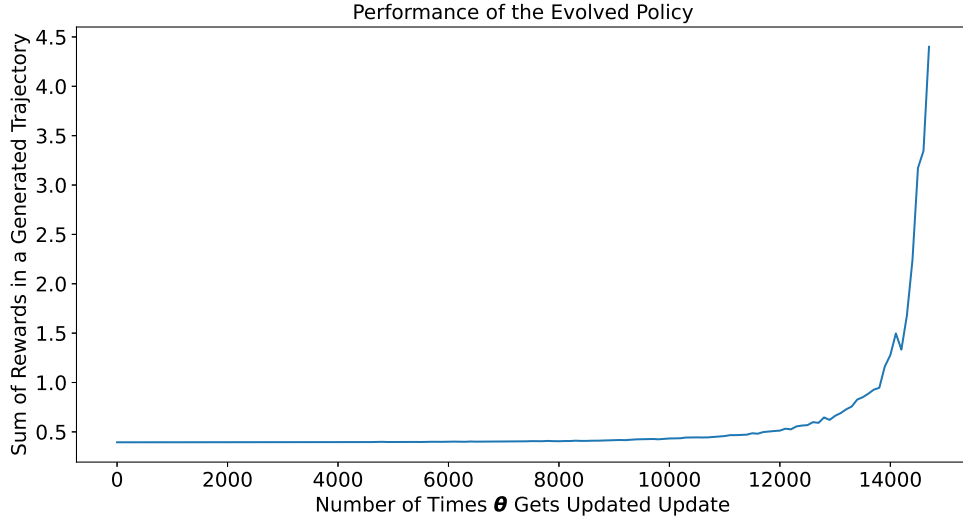


Figure 5: Performance of the Evolving Policy for Simulation Two. The procedures and hyper-parameter values are identical as those in Figure 3, except that the initial state \mathbf{x}_0 for each generated trajectory is fixed at $\mathbf{0} \in \mathbb{R}^D$.

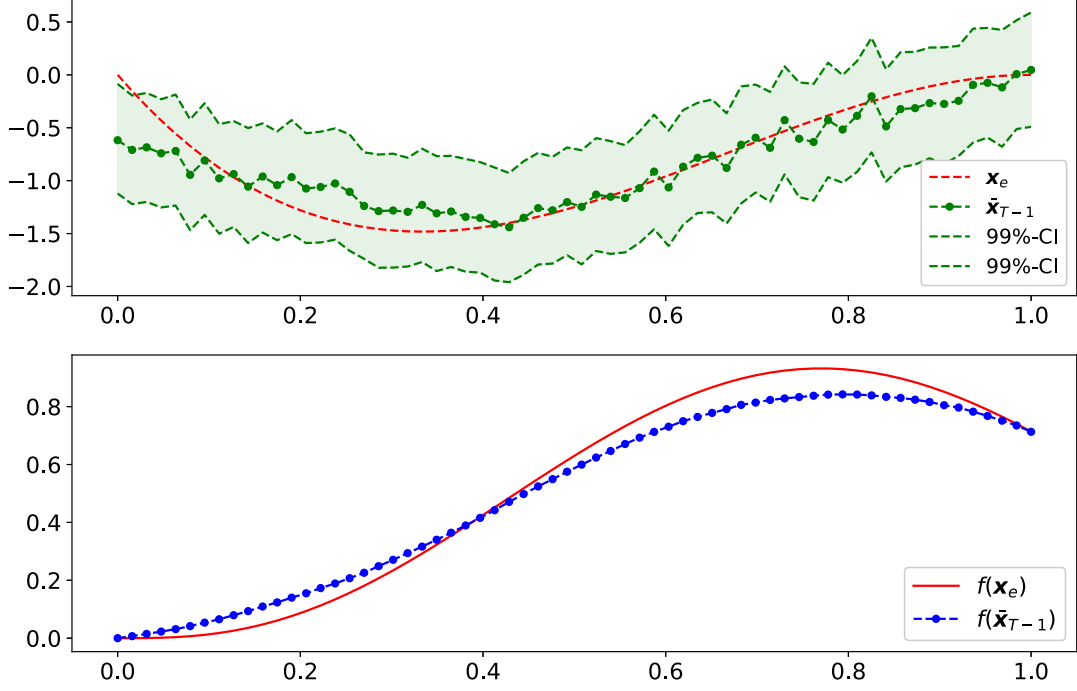


Figure 6: The Estimations and True Values for Simulation Two. The procedures for producing the plots and the symbols are the same as those in Figure 3.

Note that in Figure 6 the agent π_θ finds an approximation to $-\mathbf{x}_e$. But as we repeat this experiment for more times (each experiment requires retraining π_θ), we end up with an approximation to \mathbf{x}_e , at a chance of approximately 50%.

5.1.3 Simulation three

In the last group of simulations, we perform another experiment to illustrate that with a proper setting of the initial state’s distribution, the REINFORCE algorithm is able to find good approximations of both of the two solutions without the need to retrain the model. Suppose we are given the priori information that one solution is near $3\mathbf{x}_e/4$ and the other is near $-3\mathbf{x}_e/4$. With this information, in the θ -updating process we set initial state \mathbf{x}_0 of each trajectory as either $3\mathbf{x}_e/4$ or $-3\mathbf{x}_e/4$, each with a probability of 50%. Figure 7 shows the performance of the policy π_θ that is updated repeatedly according to the REINFORCE algorithm (21) and the performance is computed by the following procedure. (1) Use π_θ to generated $L = 1,000$ trajectories of length $T = 10$. (2) The last-step state \mathbf{x}_{T-1} in each trajectory is taken as an estimate of the solution, and hence we have 10,000 estimates, $\{\mathbf{x}_{l,T-1}\}_{l=1}^{1000}$. (3) The K-mean algorithm is then applied to divide $\{\mathbf{x}_{l,T-1}\}_{l=1}^{1000}$ to two groups. Compute the mean of each group, denoted as $\bar{\mathbf{x}}_1$ and $\bar{\mathbf{x}}_2$. (4) The performance of π_θ is computed as $(f(\bar{\mathbf{x}}_1) + f(\bar{\mathbf{x}}_2))/2$.

To test the capacity of the trained policy to find solutions to (41), similar to the previous experiment, we generate $L = 10,000$ trajectories of length $T = 10$ with the trained agent π_θ . But note that in this experiment the initial state \mathbf{x}_0 takes the value of $3\mathbf{x}_e/4$ or $-3\mathbf{x}_e/4$, each with a probability of 50%. The last-step state \mathbf{x}_{T-1} in each trajectory is taken as an estimate of the solution, and hence we have 10,000 estimates, $\{\mathbf{x}_{l,T-1}\}_{l=1}^{10000}$. The K-mean algorithm is then applied to divide $\{\mathbf{x}_{l,T-1}\}_{l=1}^{10000}$ to two groups. Then, for each group we use the bootstrapping method (same as the one in the previous experiment) to estimate the 99% confidence interval of each entry in our \mathbf{x}_e -estimate. The results are plotted in Figure 8, where the region bounded by the two blue dashed curves is the estimated 99%-confidence

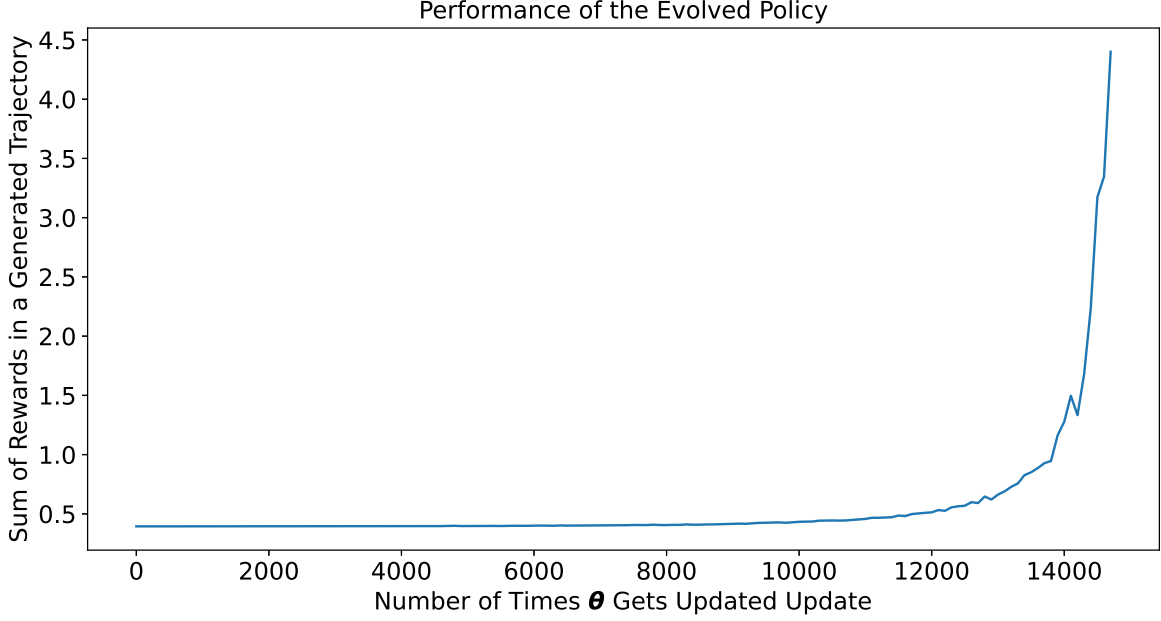


Figure 7: Performance of the Evolved Policy for Simulation Three. Comparing to Simulation One and Two, the difference lies in the distribution of the initial state \mathbf{x}_0 and the way on calculating π_θ 's performances. See the text for details.

interval based on estimates in group 2 (whose initial state is fixed at $0.75\mathbf{x}_e$). The region bounded by the two green dashed curves is for the sample means in group 1 (whose initial state is fixed at $-0.75\mathbf{x}_e$). Hence, by the definition of confidence-interval, we estimate that for each entry of the true solution lies in the shaded region with a probability of 99%.

The lower half of Figure 8 plots \mathbf{y}_e , $f(\bar{\mathbf{x}}_1)$, and $f(\bar{\mathbf{x}}_2)$, where $\bar{\mathbf{x}}_i$ denotes the mean of group- i estimates, for $i = 1$ or 2 . The R^2 -statistic between \mathbf{x}_e and $\bar{\mathbf{x}}_1$ is 97.7% and the R^2 -statistic between $-\mathbf{x}_e$ and $\bar{\mathbf{x}}_2$ is 98.4%, both of which are high. This indicates the capability of the RL algorithm to produce all the solutions to the inverse problem (41).

5.2 Parameter identification in non-linear PDE of liquid chromatography

5.2.1 Experiment Background

For the second experiment, consider the following mass balance equation of a two-component system for a fixed bed chromatography column with the Danckwerts boundary condition, which is commonly used for column chromatography ([36, 25])

$$\begin{cases} \frac{\partial C_i}{\partial t} + F \frac{\partial q_i}{\partial t} + u \frac{\partial C_i}{\partial x} = D_a \frac{\partial^2 C_i}{\partial x^2}, & x \in \mathcal{X} \equiv [0, L_1], t \in (0, T_1] \\ C_i(x, 0) = g_i(x), & x \in \mathcal{X}, t = 0 \\ u C_i(0, t) - D_a \frac{\partial C_i(0, t)}{\partial x} = u h_i(t), & x = 0, t \in (0, T_1] \\ D_a \frac{\partial C_i(L_1, t)}{\partial x} = 0, & x = L_1, t \in (0, T_1] \end{cases}, \quad (43)$$

where x is distance, t is time, and $i = 1, 2$ refers to the two components. C and q are concentration in mobile and stationary phase, respectively; $u = 0.1061$ is mobile phase velocity and $F = 0.6667$ is stationary-to-mobile phase ratio, $D_a = Lu/2N_x$ ($N_x = 2000$ denotes the number of theoretical plates) is the diffusion parameter. $L_1 = 10$ is the length of chromatographic column, and T_1 is an appropriate time point slightly larger than the dead time of chromatographic time $T_0 = L_1/u$. In this work, we set $T_1 = 1.5T_0$. Further, $g(x) =$

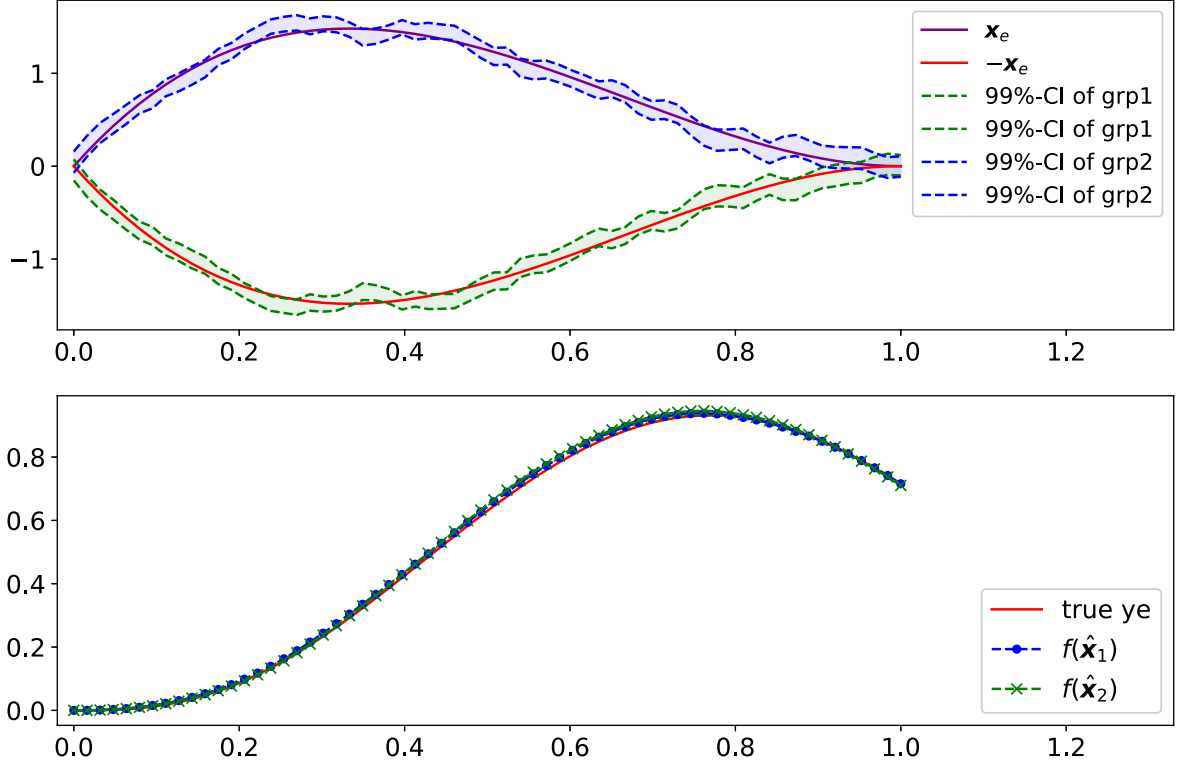


Figure 8: The Estimations and True Values

$[0, 0]_1^T$ is the initial condition and $h(t) = [5; 5] \cdot H(10 - t)$ ($H(\cdot)$ means the Heaviside step function) is the boundary condition, which describes the injection profile in the experiment.

For the numerical experiments, we focus on the case when the adsorption energy distribution is bimodal, namely the bi-Langmuir adsorption isothermis adopted

$$q_1(C_1, C_2) = \frac{a_{I,1}C_1}{1 + b_{I,1}C_1 + b_{I,2}C_2} + \frac{a_{II,1}C_1}{1 + b_{II,1}C_1 + b_{II,2}C_2}, \quad (44)$$

$$q_2(C_1, C_2) = \frac{a_{I,2}C_2}{1 + b_{I,1}C_1 + b_{I,2}C_2} + \frac{a_{II,2}C_2}{1 + b_{II,1}C_1 + b_{II,2}C_2},$$

where subscripts I and II refers to two adsorption sites with different adsorption energy.

For convenience of notation, the collection of adsorption isotherm parameters are denoted by

$$\mathbf{x} = (a_{I,1}, a_{II,1}, b_{I,1}, b_{II,1}, a_{I,2}, a_{II,2}, b_{I,2}, b_{II,2})^T. \quad (45)$$

Now, let us consider the measurement data structure. In most laboratory and industry environment, the total response $R(\mathbf{x}, t)$ is observed at the column outlet $x = L_1$ with

$$R(\mathbf{x}, t) = \sum_{i=1}^2 C_i(L_1, t), \quad (46)$$

where $C(x, t)$ is the solution of problem (43) with the bi-Langmuir adsorption isotherm model (44), and $C_i(L_1, t)$ represents the concentration of i -th component at the outlet $x = L_1$. The collected exact data at time grid $\{t_j\}_{j=1}^{T_1}$ ($T_1 = 800$) at the outlet denotes as

$$\mathbf{y}_e = \{R(\mathbf{x}, t_j)\}_{j=1}^{T_1}. \quad (47)$$

The parameter-to-measurement map $f: \mathbb{R}^8 \rightarrow \mathbb{R}_+^{T_1}$ can be expressed as

$$f(\mathbf{x}) = \mathbf{y}_e, \quad (48)$$

where the model function f is defined though (46)-(47). To be more precise, for a given parameter \mathbf{x} , a bi-Langmuir adsorption isotherm model can be constructed according to (44). Then, the concentration in mobile, i.e. C , can be obtained by solving PDE (43). Finally, the experimental data can be collected by using the designed sensor with the physical law (46) and (47). The aim in this subsection is to estimate adsorption isotherm parameters \mathbf{x} from the time series database \mathbf{y}_e and the integrated mathematical model (48) by the RL.

5.2.2 The Inverse Problem to be Solved by REINFORCE-IP

Since there is no analytical expression for the forward function f in (48), we approximate it with a neural network \hat{f} using ²⁰ 160,000 samples of (the 8 parameters \mathbf{x} , the injection profile \mathbf{h} with 2 entries²¹, and the corresponding total response \mathbf{y}). The samples of (\mathbf{x}, \mathbf{h}) are uniformly randomly drawn from $(0, 100)^8 \times (0, 30)^2$, and the samples of \mathbf{y} are computed using (\mathbf{x}, \mathbf{h}) -samples by the forward system described in the previous subsection. The testing R^2 score of \hat{f} is above 95%, indicating that it is a good approximation of f .

The inverse problem we will use REINFORCE-IP to solve is

$$\hat{f}(\mathbf{x}, \mathbf{h}) + \boldsymbol{\epsilon} = \mathbf{y}^\delta, \quad (49)$$

where $\mathbf{y}^\delta = \hat{f}(\mathbf{x}_e) + \boldsymbol{\epsilon}$, \mathbf{x}_e is randomly generated and its value is shown in Table 2, \mathbf{h} is the randomly generated projection profile that is considered to be a known parameter (the randomly drawn value is $[10, 21]$), and $\boldsymbol{\epsilon}$ is a mean-zero noise.

Similar as before, we assume that a set $\{\mathbf{y}_k^\delta\}_{k=1}^{100}$ of noised signals are available, where for each k , \mathbf{y}_k^δ is obtained by first randomly shifting²² the entries in the vector $\mathbf{y}_e = \hat{f}(\mathbf{x}_e, \mathbf{h})$ by 1 unit to obtain $\mathbf{y}_k^{\text{shift}}$, and then we add an artificial noise to it:

$$\mathbf{y}_k^\delta = \mathbf{y}_k^{\text{shift}} + \boldsymbol{\epsilon}_k,$$

where $\boldsymbol{\epsilon}_k$ is a vector of independent mean-zero normal random variables with standard deviations equal to $1\% \mathbf{y}_k^{\text{shift}}$. According to [31], the shift error is one of the major error in real-world experiments, and hence $\mathbf{y}_k^{\text{shift}}$ need to be taken into account. Moreover, in our simulations, all \mathbf{y}_k are re-arranged at the same time grids by using the spline technique because in general, the time grids of numerical solution of PDE (48) do not fit the time grids of the observation data.

5.2.3 The Experiment and Results

Since there is no prior information to use, the regularizer $\Omega(\mathbf{x})$ is set as 0. Conforming to (38), we define the reward function as

$$R(\mathbf{x}, \mathbf{a}) := \frac{1}{\sum_{k=1}^{100} (f(\mathbf{x} + \mathbf{a}) - \mathbf{y}_k^\delta)^2 / (100 \times 800) + 0.001}, \quad (50)$$

where 800 is the dimension of \mathbf{y}_k^δ . As stated in Section 5.1, we construct the policy $\pi_\theta(\cdot|\mathbf{x})$ as a multivariate normal distribution whose mean and standard deviation are outputs from a neural network \mathcal{N}_θ . Values of the hyper-parameters are selected through cross validation and are reported in Table 1.

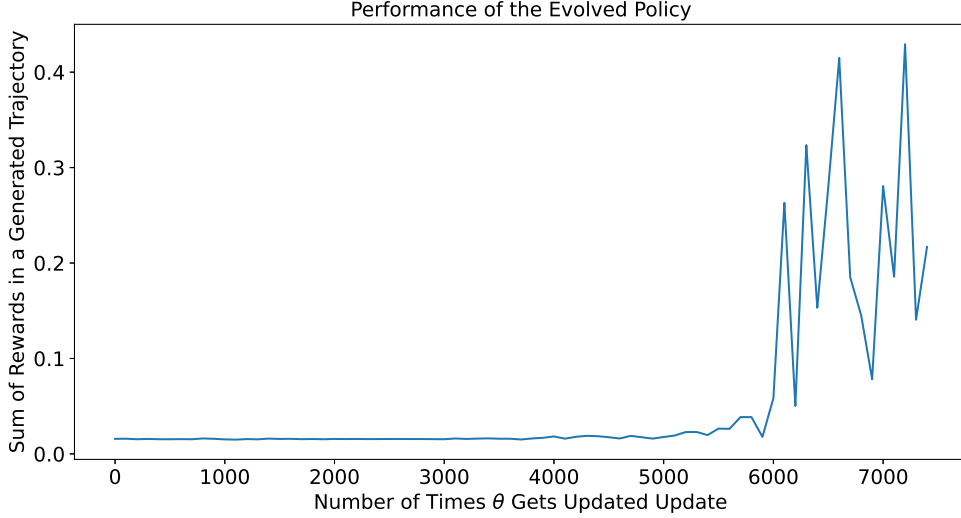
²⁰This feed-forward neural network \hat{f} is trained in the same way as F_{fwn} in [31, Section 3.1].

²¹ \mathbf{h} is the finite analog of injection function $h(t)$ in PDE (43).

²²Denote $\mathbf{y}_e := \hat{f}(\mathbf{x}_e) = [y_0, y_1, \dots, y_{799}]$. Then, with a probability of 50%, $\mathbf{y}_k^{\text{shift}} = [y_1, y_2, \dots, y_{799}, 0]$ (shifted to the left for 1 unit). With a probability of 50%, $\mathbf{y}_k^{\text{shift}} = [0, y_0, y_1, \dots, y_{798}]$ (shifted to the right for 1 unit).

Table 1: Structure of \mathcal{N}_θ and Hyper-parameter Values

T	α	Hidden Layers-Nodes	Activation	β	Learning Rate
10	0.1	(128, 64, 16)	relu	0.1	0.001

Figure 9: Performance of the Evolved Policy π_θ .

We repeatedly train the neural net until the sum of rewards in a trajectory generated by the policy stops improving²³ or the total number of θ -updates exceeds 12,500, which one comes first. Figure 9 shows the performance of the policy π_θ that is updated repeatedly in the training process.

Similar to the previous experiments, with the trained actor π_θ , we generate $L = 1,000$ trajectories of length $T = 10$, each starting from the fixed initial state $[50, 50, \dots, 50]$, and take the last state $\mathbf{x}_{l,T-1}$ in each trajectory as an estimate of \mathbf{x}_e . The mean $\bar{\mathbf{x}}_{T-1}$ of these L estimates, and the estimated 99% confidence interval obtained by bootstrapping from these estimates, are reported in Table 2. From the table we see that the entries of $\bar{\mathbf{x}}_{T-1}$ are close to \mathbf{x}_e , except entry-2, 4, and 5. These three entries in \mathbf{x}_e are beyond the estimated 99% confidence interval. This happens because this chromatography problem has multiple solutions, and in this experiment REINFORCE-IP finds one different from \mathbf{x}_e .

The forward signals, $f(\mathbf{x}_e)$ and $f(\bar{\mathbf{x}}_{T-1})$ (plotted in Figure 10), are close to each other with a R^2 between them as high as 91.8%, indicating that the REINFORCE algorithm is successful for this experiment.

6 Conclusion and outlook

In this work, by using the reinforcement learning, we developed a novel regularization algorithm, called REINFORCE-IP, for solving nonlinear operator equations. Our numerical experiments show that REINFORCE-IP is an efficient algorithm exhibiting the merits that it can escape from local minimum of the loss function (see Figure 1 and 2) and to identify multi-solutions (see Figure 8). Our theoretical contribution consists of the rigorous proof of the convergence of well-known machine learning algorithm – REINFORCE. It should be noted that REINFORCE is one of the early RL algorithms that apply function approxi-

²³Specifically, we log the sum of rewards in a trajectory every 100 updates of θ . If the logged value does not improve for 10 logs, then we stop training.

Table 2: Estimations By REINFORCE-IP. $\bar{\mathbf{x}}_{T-1}$ represents the mean of \mathbf{x}_e -estimates. The row of CI-LB stores the lower bounds of 99% confidence interval, and the row of CI-UP stores the upper bounds of 99% confidence interval. Column i corresponds to the i^{th} entry, for $i \in \{1, 2, \dots, 8\}$.

	1	2	3	4	5	6	7	8
\mathbf{x}_e	50.0	43.0	48.0	40.0	59.0	50.0	51.0	49.0
$\bar{\mathbf{x}}_{T-1}$	48.1	49.7	48.6	50.0	55.3	48.9	54.2	50.3
99%CI-LB	42.5	43.8	42.9	43.9	49.8	42.9	49.0	44.4
99%CI-UB	53.6	55.8	54.7	56.6	61.1	54.7	59.6	56.0

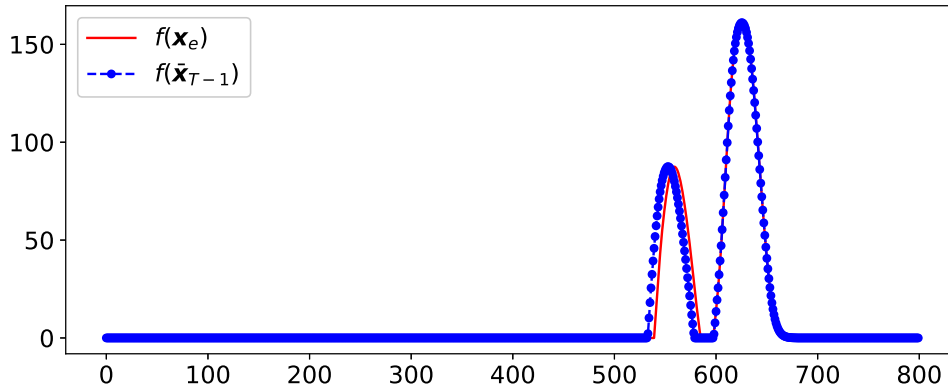


Figure 10: The Estimations and True Values

mators such as π_{θ} , which makes it powerful dealing with an infinite state space. However, the adopted Monte Carlo mechanism leads to a high variance of the estimate $\hat{\nabla} J_{\theta}$, causing a slow learning process even if a baseline is used (see [29, Section 13.4 and 13.5]). This deficiency is avoided by the later developed and more powerful actor-critic methods (see e.g., [5, 20, 21, 22, 32, 17, 29]), where an actor refers to π_{θ} and a critic refers to a function approximator for $J_T(\theta)$. To our knowledge, the performance of these actor-critic methods on the general-type inverse problem (1) is still unknown and to be investigated, and we leave this topic for future works.

References

- [1] J. Baumeister. Deconvolution of appearance potential spectra. In *Methoden Verfahren Mathematical Physics*, volume 35, pages 1–13. Frankfurt am Main: Peter Lang, 1991.
- [2] S. Bhatnagar and V. Borkar. A two timescale stochastic approximation scheme for simulation-based parametric optimization. *Probability in the Engineering and Informational Sciences*, 12(4):519–531, 1998.
- [3] P. Billingsley. *Probability and Measure*. John Wiley and Sons, 3rd edition, 1995.
- [4] V. Borkar. *Stochastic Approximation: A Dynamical Systems Viewpoint*. Hindustan Book Agency Gurgaon, 2022.
- [5] V. Borkar and V. Konda. The actor-critic algorithm as multi-time-scale stochastic approximation. *Sadhana*, 22:525–543, 1997.

- [6] V. Borkar and S. Meyn. The o.d.e. method for convergence of stochastic approximation and reinforcement learning. *SIAM Journal on Control and Optimization*, 38(2):447–469, 2000.
- [7] L. Bottou. Stochastic gradient learning in neural networks. *Proceedings of Neuro-Nimes*, 1991.
- [8] Z. Dai. Local regularization methods for inverse Volterra equations applicable to the structure of solid surfaces. *Journal of Integral Equations and Applications*, 25(2):223–252, 2013.
- [9] P. Dell’Aversana. Reinforcement learning in optimization problems: Applications to geophysical data inversion. *AIMS Geosciences*, 8(3):488–502, 2022.
- [10] R. Douc, E. Moulines, P. Priouret, and P. Soulier. *Markov Chain*. Springer Cham, 1st edition, 2018.
- [11] Y. Fukuda. Appearance potential spectroscopy (APS): old method, but applicable to study of nano-structures. *Analytical Sciences*, 26(2):187–197, 2010.
- [12] D. Gerth, B. Hofmann, S. Birkholz, S. Koke, and G. Steinmeyer. Regularization of an autoconvolution problem in ultrashort laser pulse characterization. *Inverse Problems in Science and Engineering*, 22(2):245–266, 2014.
- [13] R. Gorenflo and B. Hofmann. On autoconvolution and regularization. *Inverse Problems*, 10(2):353–373, 1994.
- [14] B. Hofmann and R. Plato. On ill-posedness concepts, stable solvability and saturation. *Journal of Inverse and Ill-posed Problems*, 26(2):287–297, 2018.
- [15] B. Hofmann and O. Scherzer. Local ill-posedness and source conditions of operator equations in Hilbert spaces. *Inverse Problems*, 14(5):1189–1206, 1998.
- [16] M. Holzleitner, L. Gruber, J. Arjona-Medina, J. Brandstetter, and S. Hochreiter. *Convergence Proof for Actor-Critic Methods Applied to PPO and RUDDER*, pages 105–130. Springer Berlin Heidelberg, Berlin, Heidelberg, 2021.
- [17] M. Hong, H. Wai, Z. Wang, and Z. Yang. A two-timescale stochastic algorithm framework for bilevel optimization: Complexity analysis and application to actor-critic. *SIAM Journal on Optimization*, 33(1):147–180, 2023.
- [18] P. Karmakar and S. Bhatnagar. Two time-scale stochastic approximation with controlled markov noise and off-policy temporal-difference learning. *Mathematics of Operations Research*, 43(1):130–151, 2018.
- [19] A. Klenke. *Probability Theory*. Springer London, 2nd edition, 2013.
- [20] V. Konda and V. Borkar. Actor-critic-type learning algorithms for markov decision processes. *SIAM Journal on Control and Optimization*, 38(1):94–123, 1999.
- [21] V. Konda and J. Tsitsiklis. Actor-critic algorithms. In S. Solla, T. Leen, and K. Müller, editors, *Advances in Neural Information Processing Systems*, volume 12. MIT Press, 1999.
- [22] V. R. Konda and T. J. N. On actor-critic algorithms. *SIAM Journal on Control and Optimization*, 42(4):1143–1166, 2003.

- [23] H. Le, Y. Wang, A. D. Gotmare, S. Savarese, and S. C. H. Hoi. Coderl: Mastering code generation through pretrained models and deep reinforcement learning. In *Advances in Neural Information Processing Systems*, volume 35, pages 21314–21328. Curran Associates, Inc., 2022.
- [24] Y. Li. Deep reinforcement learning: An overview. <http://arxiv.org/abs/1701.07274>, 2018.
- [25] G. Lin, Y. Zhang, X. Cheng, M. Gulliksson, P. Forssén, and T. Fornstedt. A regularizing Kohn-Vogelius formulation for the model-free adsorption isotherm estimation problem in chromatography. *Applicable Analysis*, 97:13–40, 2018.
- [26] M. Puth, M. Neuhäuser, and G. D. Ruxton. On the variety of methods for calculating confidence intervals by bootstrapping. *Journal of Animal Ecology*, 84:892–897, 2015.
- [27] F. Santosa and L. Anderson. Bayesian sequential optimal experimental design for linear regression with reinforcement learning. In *2022 21st IEEE International Conference on Machine Learning and Applications (ICMLA)*, pages 641–646, 2022.
- [28] B. Sridharan, S. Mehta, Y. Pathak, and U. Priyakumar. Deep reinforcement learning for molecular inverse problem of nuclear magnetic resonance spectra to molecular structure. *The Journal of Physical Chemistry Letters*, 13(22):4924–4933, 1992.
- [29] R. Sutton and A. Barto. *Reinforcement Learning: An Introduction*. The MIT Press, 2018.
- [30] R. J. Williams. Simple statistical gradient-following algorithms for connectionist reinforcement learning. *Machine Learning*, 8(3-4):229–256, 1992.
- [31] C. Xu and Y. Zhang. Estimating adsorption isotherm parameters in chromatography via a virtual injection promoting double feed-forward neural network. *Journal of Inverse and Ill-Posed Problems*, 30(5):693–712, 2022.
- [32] T. Xu, Z. Yang, Z. Wang, and Y. Liang. Doubly robust off-policy actor-critic: Convergence and optimality. In M. Meila and T. Zhang, editors, *Proceedings of the 38th International Conference on Machine Learning*, volume 139 of *Proceedings of Machine Learning Research*, pages 11581–11591. PMLR, 18–24 Jul 2021.
- [33] J. Yang, C. Xu, and Y. Zhang. Reconstruction of the s-wave velocity via mixture density networks with a new rayleigh wave dispersion function. *IEEE Transactions on Geoscience and Remote Sensing*, 60:1–13, 2022.
- [34] J. Zhang, J. Kim, B. O’Donoghue, and S. Boyd. Sample efficient reinforcement learning with reinforce. In *Proceedings of the AAAI Conference on Artificial Intelligence*, volume 35, pages 10887–10895, 2021.
- [35] Y. Zhang and C. Chen. Stochastic asymptotical regularization for linear inverse problems. *Inverse Problems*, 39:015007, 2023.
- [36] Y. Zhang, G. Lin, P. Forssén, M. Gulliksson, T. Fornstedt, and X. Cheng. A regularization method for the reconstruction of adsorption isotherms in liquid chromatography. *Inverse Problem*, 32(10):105005, 2016.
- [37] T. Zhao, H. Hachiya, G. Niu, and M. Sugiyama. Analysis and improvement of policy gradient estimation. *Neural Networks*, 26:118–129, 2012.
- [38] B. Zoph and Q. V. Le. Neural architecture search with reinforcement learning, 2017.

7 Appendix

Appendix 1 - Used lemmas in the article

Lemma 3. (Gronwall inequality, [4, Lemma B.1]) For continuous $u(\cdot), v(\cdot) \geq 0$ and scalars $C, K, T \geq 0$,

$$u(t) \leq C + K \int_0^t u(s)v(s)ds \quad \text{for all } t \in [0, T],$$

implies

$$u(t) \leq Ce^{K \int_0^t v(s)ds}, t \in [0, T]$$

Remark 3. From the proof given in [4, Lemma B.1]), Lemma 3 still holds when C is dependent on T .

Lemma 4. (Discrete Gronwall Inequality, [4, Lemma B.2]) Let $\{x_n, n \geq 0\}$ (resp. $\{a_n, n \geq 0\}$) be non-negative (resp. positive) sequences and $C, L \geq 0$ be scalars such that for all n ,

$$x_{n+1} \leq C + L \left(\sum_{m=0}^n a_m x_m \right).$$

Then, $x_{n+1} \leq Ce^{Ls_n}$, where $s_n = \sum_{m=0}^n a_m$ for each non-negative integer n .

Lemma 5. ([4, Theorem C.3]) Suppose $\{X_n\}_{n=0}^\infty$ is a martingale with respect to $\{\mathcal{F}_n\}$, defined on the probability space (Ω, \mathcal{F}, P) . Also assume that $\mathbb{E}[X_n^2] < \infty$. Then,

- $\sum_{n=0}^\infty \mathbb{E}[(X_{n+1} - X_n)^2 | \mathcal{F}_n] < +\infty$ implies that almost surely $\{X_n\}_{n=0}^\infty$ converges.
- $\sum_{n=0}^\infty \mathbb{E}[(X_{n+1} - X_n)^2 | \mathcal{F}_n] = +\infty$ implies that

$$X_n = o \left(\sum_{m=1}^{n-1} \mathbb{E}[(X_{m+1} - X_m)^2 | \mathcal{F}_m] \right), \text{ a.s.}$$

Appendix 2: Proof to the implication in Step 1 of Lemma 2's proof

The following lemma will be used for proving the implication stated in Step 1 of Lemma 2's Proof.

Lemma A.1 Consider the ODE $\dot{x}(t) = f(x(t))$, where $f : \mathbb{R}^d \rightarrow \mathbb{R}^d$ is Lipschitz with the Lipschitz constant $L_f > 0$. Assume that $x_1(\cdot)$ and $x_2(\cdot)$ are two solutions to the ODE, then for any $\Delta > 0$ and any $t \in [0, \Delta]$ we have

$$\|x_1(t) - x_2(t)\| \leq \|x_1(0) - x_2(0)\| e^{L_f \Delta}.$$

Proof. Note that

$$\begin{aligned} \|x_1(t) - x_2(t)\| &= \left\| \int_0^t [f(x_1(s)) - f(x_2(s))]ds + (x_1(0) - x_2(0)) \right\| \\ &\leq \int_0^t \|f(x_1(s)) - f(x_2(s))\|ds + \|x_1(0) - x_2(0)\| \\ &\leq L_f \int_0^t \|x_1(s) - x_2(s)\|ds + \|x_1(0) - x_2(0)\|. \end{aligned}$$

Hence, by Gronwall inequality (see Lemma 3 in Appendix 1), we have for any $t \in [0, \Delta]$,

$$\|x_1(t) - x_2(t)\| \leq \|x_1(0) - x_2(0)\| e^{L_f \Delta}.$$

□

Proof to the Implication in Step 1. Suppose that Eq. (28) holds. Our goal is to prove Eq. (24). That is, for any fixed $\Delta > 0$,

$$\lim_{s \rightarrow +\infty} \left(\sup_{t \in [s, s+\Delta]} \|\bar{\theta}(t) - \theta^s(t)\| \right) = 0, \quad \text{for any fixed } \Delta > 0.$$

We follow Step (L1) to (L3) to prove it.

Step (L1) We prove that

$$\lim_{n \rightarrow +\infty} \left(\sup_{t \in [s_n, s_n+\Delta]} \|\bar{\theta}(t) - \theta^{s_n}(t)\| \right) = 0.$$

Proof. By Eq. (28), we have

$$\lim_{n \rightarrow +\infty} \left(\sup_{t \in [s_n, [s_n+\Delta+1]^-]} \|\bar{\theta}(t) - \theta^{s_n}(t)\| \right) = 0, \quad \text{for any fixed } \Delta > 0.$$

We will show that when n is large enough,

$$s_n + \Delta \leq [s_n + \Delta + 1]^-, \quad (51)$$

which further implies

$$\begin{aligned} & \lim_{n \rightarrow +\infty} \left(\sup_{t \in [s_n, s_n+\Delta]} \|\bar{\theta}(t) - \theta^{s_n}(t)\| \right) \\ & \leq \lim_{n \rightarrow +\infty} \left(\sup_{t \in [s_n, [s_n+\Delta+1]^-]} \|\bar{\theta}(t) - \theta^{s_n}(t)\| \right) \\ & = 0. \end{aligned}$$

Now, to finish Step (L1) it remains to prove (51) is true when n is large enough. By Point 3 in Assumption 1, $\lim_{n \rightarrow +\infty} a_n = 0$. Therefore, there exists $N > 0$ such that whenever $n > N$, $a_n < 1$. Now, suppose $n > N$ and let k denote the positive integer such that $s_k := [s_n + \Delta + 1]^-$. Then,

$$\begin{aligned} s_n + \Delta + 1 - [s_n + \Delta + 1]^- & \leq [s_n + \Delta + 1]^+ - [s_n + \Delta + 1]^- \\ s_n + \Delta + 1 - [s_n + \Delta + 1]^- & \leq s_{k+1} - s_k \\ s_n + \Delta + 1 - [s_n + \Delta + 1]^- & \leq a_k \\ s_n + \Delta - [s_n + \Delta + 1]^- & \leq -1 + a_k \\ s_n + \Delta - [s_n + \Delta + 1]^- & \leq 0 \end{aligned}$$

where the last inequality is due to $k \geq n > N$ (by the definition of s_k) and hence $-1 + a_k < 0$. This proves Eq. (51) and finishes the proof for the equality in Step (L1). \square

Step (L2). We prove that when s is large enough,

$$\sup_{t \in [s, s+\Delta]} \|\bar{\theta}(t) - \theta^s(t)\| \leq \sup_{t \in [[s]^-, [s]^- + \Delta + 1]} \|\bar{\theta}(t) - \theta^{[s]^-}(t)\| (1 + e^{L_g(\Delta+1)}).$$

Proof. Recall that $\lim_{n \rightarrow +\infty} a_n = 0$. Let $N > 0$ denote the threshold such that whenever $n \geq N$, $a_n < 1$. For any $s \geq s_N$, let k denote the non-negative integer such that $[s]^- = s_k$. Then, $k \geq N$ and

$$s - [s]^- \leq [s]^+ - [s]^- = s_{k+1} - s_k = a_k < 1,$$

which implies

$$s \leq [s]^- + 1 \Rightarrow s + \Delta \leq [s]^- + \Delta + 1. \quad (52)$$

This result is used to derive the second inequality of the following.

$$\begin{aligned} \sup_{t \in [s, s+\Delta]} \|\bar{\boldsymbol{\theta}}(t) - \boldsymbol{\theta}^s(t)\| &\leq \sup_{t \in [s, s+\Delta]} \|\bar{\boldsymbol{\theta}}(t) - \boldsymbol{\theta}^{[s]^-}(t)\| + \sup_{t \in [s, s+\Delta]} \|\boldsymbol{\theta}^{[s]^-}(t) - \boldsymbol{\theta}^s(t)\| \\ &\leq \sup_{t \in [[s]^- , [s]^- + \Delta + 1]} \|\bar{\boldsymbol{\theta}}(t) - \boldsymbol{\theta}^{[s]^-}(t)\| + \sup_{t \in [s, s+\Delta]} \|\boldsymbol{\theta}^{[s]^-}(t) - \boldsymbol{\theta}^s(t)\| \end{aligned} \quad (53)$$

Now, we derive an upper bound for the second sup-term, $\sup_{t \in [s, s+\Delta]} \|\boldsymbol{\theta}^{[s]^-}(t) - \boldsymbol{\theta}^s(t)\|$. Define $y_{[s]^-}(t) := \boldsymbol{\theta}^{[s]^-}(t + s)$ and $y_s(t) := \boldsymbol{\theta}^s(t + s)$. Then, $y_{[s]^-}(t)$ and $y_s(t)$ are solutions to ODE (25) since

$$\begin{aligned} \dot{y}_{[s]^-}(t) &= \dot{\boldsymbol{\theta}}^{[s]^-}(t + s) = g(\boldsymbol{\theta}^{[s]^-}(t + s)) = g(y_{[s]^-}(t)); \\ \dot{y}_s(t) &= \dot{\boldsymbol{\theta}}^s(t + s) = g(\boldsymbol{\theta}^s(t + s)) = g(y_s(t)). \end{aligned}$$

The definitions of $y_{[s]^-}(t)$ and $y_s(t)$ imply the second line in the following

$$\begin{aligned} \sup_{t \in [s, s+\Delta]} \|\boldsymbol{\theta}^{[s]^-}(t) - \boldsymbol{\theta}^s(t)\| &= \sup_{t \in [0, \Delta]} \|\boldsymbol{\theta}^{[s]^-}(t + s) - \boldsymbol{\theta}^s(t + s)\| \\ &= \sup_{t \in [0, \Delta]} \|y_{[s]^-}(t) - y_s(t)\| \\ &\leq \|y_{[s]^-}(0) - y_s(0)\| e^{L_g \Delta}, \text{ by Lemma A.1,} \\ &= \|\boldsymbol{\theta}^{[s]^-}(s) - \boldsymbol{\theta}^s(s)\| e^{L_g \Delta} \\ &= \|\boldsymbol{\theta}^{[s]^-}(s) - \bar{\boldsymbol{\theta}}(s)\| e^{L_g \Delta}, \text{ By } \boldsymbol{\theta}^s\text{-definition,} \\ &\leq \sup_{t \in [[s]^- , [s]^- + \Delta + 1]} \|\bar{\boldsymbol{\theta}}(t) - \boldsymbol{\theta}^{[s]^-}(t)\| e^{L_g \Delta}, \end{aligned}$$

where the last inequality is due to the fact that when s is sufficiently large, $s \in [[s]^- , [s]^- + \Delta + 1]$ by (52). Plugging this result to (53) proves Step (L2). \square

Step (L3). Take the limit of both sides of the inequality in Step (L2):

$$\lim_{s \rightarrow +\infty} \sup_{t \in [s, s+\Delta]} \|\boldsymbol{\theta}^{[s]^-}(t) - \boldsymbol{\theta}^s(t)\| \leq \lim_{s \rightarrow +\infty} \sup_{t \in [[s]^- , [s]^- + \Delta + 1]} \|\bar{\boldsymbol{\theta}}(t) - \boldsymbol{\theta}^{[s]^-}(t)\| (1 + e^{L_g(\Delta+1)}) = 0,$$

where the equality is by Step (L1). This finishes Step (L3) and hence the whole proof to the implication in Step 1 of Lemma 2's proof.

Appendix 3. Conditions that ensures the existence of a stationary distribution of a Markov chain

Let $\{X_k\}_{k=0}^\infty$ be a Markov chain defined on a measurable space $(\mathbf{X}, \mathcal{X})$. Denote its Markov kernel by P . The invariant distribution of $\{X_k\}$ (also called a stationary or a normalized invariant measure), if exists, refers to a probability measure μ on $(\mathbf{X}, \mathcal{X})$ satisfying

$$\mu P = \mu \text{ and } \mu(\mathbf{X}) = 1.$$

Sufficient but possibly unnecessary conditions for the existence of a unique invariant distribution can be found in [10, Section 2.1.2], which requires \mathbf{X} to be a complete and separable metric space and [10, Section 2.1.2, H2.1.8] as copied below.

(1) There exists a measurable function $K : \mathbf{Z} \rightarrow \mathbb{R}_+$ such that for all $(x, y, z) \in \mathbf{X} \times \mathbf{X} \times \mathbf{Z}$,

$$d(f(x, z), f(y, z)) \leq K(z)d(x, y), \text{ and} \\ \mathbb{E}[\max\{\log K(Z_1), 0\}] < \infty, \quad \mathbb{E}[\log K(Z_1)] < 0,$$

where

- d denotes the metric on \mathbf{X} .
- $(\mathbf{Z}, \mathcal{Z})$ is a measurable space;
- $\{Z_k\}_{k=0}^\infty$ is a sequence of i.i.d. random variables taking values in \mathbf{Z} ;
- $f : \mathbf{X} \times \mathbf{Z} \rightarrow \mathbf{X}$ is a $\mathcal{X} \otimes \mathcal{Z}$ - \mathcal{X} measurable map such that $X_k = f(X_{k-1}, Z_k)$. Note that its existence is guaranteed by the fact that \mathcal{X} is finitely generated (since \mathbf{X} is separable) and by Theorem 1.3.6 in [10].

(2) There exists $x_0 \in \mathbf{X}$ such that

$$\mathbb{E}[\log^+ d(x_0, f(x_0, Z_1))] < \infty.$$

Appendix 4. Notations

Notation	Description	Reference
\mathbb{Z}^+	The set of positive integers.	
\mathbf{y}_k^δ	The k^{th} observed sample of \mathbf{y}^δ .	(1).
$\Omega(\mathbf{x})$	The regularization term.	(2).
α, β	The non-negative regularization coefficients.	(2) and (3).
$\pi_\theta(\cdot \mathbf{x})$	A probability density of the action \mathbf{a} given the current state \mathbf{x} .	Near (4).
d^{π_θ}	The invariant distribution of the Markov chain $\{\mathbf{x}_t\}_{t=0}^{+\infty}$ generated by following policy π_θ .	First appears in 3 but explained in Section 2.2.
\mathbf{x}_t	The state in step t in a trajectory.	(5).
\mathbf{a}_t	The action taken in step t in a trajectory.	(5).
T	The trajectory length $\{\mathbf{x}_t\}_{t=0}^{T-1}$.	(5).
$J_T(\theta)$	The expected sum of rewards obtained in a trajectory of length T generated following the policy π_θ .	(5).
$\mathbb{E}_{\mathbf{x}_t, \mathbf{a}_t}[\cdot \pi_\theta]$	The expectation over $(\mathbf{x}_t, \mathbf{a}_t)$ given that they are the step t state-action pair in a trajectory generated by π_θ . This expectation is also determined by the initial state \mathbf{x}_0 . But we consider the initial state's distribution as fixed.	(5).
$\overline{U(\mathbf{0}; B_1)}$	$\{\theta \mid \theta \in \mathbb{R}^d, \ \theta\ \leq B_1\}$.	Assumption 2.
$\nabla J_T(\theta)$	$\frac{\partial J_T \theta}{\partial \theta}$.	(14).
$\hat{\nabla} J_T(\theta)$	Sample estimate of $\nabla J_T \theta$.	(21).
$g(\cdot)$	A Lipschitz map from \mathbb{R}^d to \mathbb{R}^d , with the Lipschitz coefficient of L_g .	Assumption 1.
M_{n+1}	$\hat{\nabla} J_T(\theta_n) - \nabla J_T(\theta_n)$.	(22).
a_n	The updating step size for $\{\theta_n\}$.	(21).

s_n	$s_n := \sum_{i=0}^{n-1} a_i$ for any $n > 0$ and $s_0 := 0$.	Lemma 2.
$\{\boldsymbol{\theta}_n\}_{n=0}^{+\infty}$	The iterate sequence.	(22) or (21).
$\bar{\boldsymbol{\theta}}(\cdot)$	$\bar{\boldsymbol{\theta}}(t) := \lambda_t \boldsymbol{\theta}_n + (1 - \lambda_t) \boldsymbol{\theta}_{n+1}$ for $t \in [s_n, s_{n+1}]$, where	Lemma 2.
	$\lambda_t := \frac{s_{n+1}-t}{s_{n+1}-s_n} \in [0, 1]$.	
$\boldsymbol{\theta}^s(\cdot)$	A solution to ODE (25) with $\boldsymbol{\theta}^s(s) = \bar{\boldsymbol{\theta}}(s)$.	Lemma 2.
